



Physical and biological processes driving seasonal variability of Nitrate budget and biological productivity in the Gabon-Congo upwelling system

Landry Junior Mbang Essome^{1,2}, Gaël Alory¹, Casimir Yelognissé Da-Allada^{2,3,5}, Isabelle Dadou¹, Roy Dorgeless Ngakala^{3,4}, and Guillaume Morvan¹

¹Université de Toulouse, LEGOS (CNES/CNRS/IRD/UT), Toulouse, France

²Laboratoire de Géosciences, de l'Environnement et Applications, Université Nationale des Sciences Technologies, Ingénierie et Mathématiques, Abomey, Benin

³Department of Oceanography and Applications, International Chair in Mathematical Physics and Applications, University of Abomey-Calavi, Cotonou, Benin

⁴Department of Oceanography and Environment, Institut National de Recherche en Sciences Exactes et Naturelles, Pointe-Noire, Congo

⁵Laboratoire d'Hydrologie Marine et Côtière, Institut de Recherches Halieutiques et Océanologiques du Bénin, Cotonou, Benin

Correspondence: Landry Junior Mbang Essome (landrymbangessome@gmail.com)

Received: 15 October 2025 – Discussion started: 11 November 2025

Revised: 26 March 2026 – Accepted: 26 March 2026 – Published: 22 April 2026

Abstract. The Gabon-Congo upwelling system, located in the southeastern Gulf of Guinea, is a highly productive marine ecosystem influenced by both local and remote physical forcing. This study investigates the seasonal variability of the nitrate budget and biological productivity in this region using a high-resolution (1/36°) coupled physical-biogeochemical simulation with the NEMO-PISCES model. The analysis highlights the relative contributions of physical and biological processes in modulating nitrate concentrations in both the mixed layer and the euphotic zone. Results reveal a semi-annual cycle of nitrate, with two upwelling periods (May–August and December) and two downwelling periods (January–April and October–November). These cycles are primarily driven by the passage of coastal trapped waves (CTWs) forced by equatorial Kelvin waves, inducing vertical thermocline displacements and regulating nitrate availability in the euphotic zone.

The nitrate budget analysis shows that the vertical diffusion linked to internal tide and local wind, and vertical advection linked to the CTWs, are the dominant process supplying nitrate to the mixed layer during the main upwelling season. However, near the Congo River mouth (5.5–6° S), the

horizontal advection plays a key role, supplying significant amounts of nitrate through the river plume. In the lower euphotic layer, the vertical mixing contributes to the nitrate loss during the upwelling but becomes a source of nitrate during the downwelling periods. The seasonal cycle of the chlorophyll *a* (CHL_a) concentration follows that of nitrate, confirming that the primary production in this region is mainly driven by nitrate availability. The study also highlights the role of the Angola Current in transporting low-nitrate waters from the Equatorial Undercurrent, which influences the nitrate and CHL_a balance in the Gabon-Congo upwelling system.

These findings provide new insights into the mechanisms governing nutrient dynamics and biological productivity in the Gabon-Congo upwelling system. Understanding these processes is crucial for assessing the impact of climate variability on the regional marine ecosystems and fisheries.

1 Introduction

The Eastern Boundary Upwelling Systems (EBUS) are the most productive areas in the global ocean in terms of biological resources, hosting almost 20 % of the world's fisheries (Chavez and Messié, 2009; Messié and Chavez, 2015), even though they only represent around 1 % of the world's ocean surface (Fréon et al., 2009). They are therefore an important economic support for the countries bordering these areas (Carr, 2002). EBUS are controlled by wind stress blowing parallel to the coast, generating an offshore Ekman transport leading to coastal upwelling of cold and nutrient-rich waters, which trigger primary production in the euphotic layer, with increased surface chlorophyll *a* (CHL_a) concentration visible on satellite images (e.g. Gutknecht et al., 2013). Besides their ecological richness, EBUS act as active interfaces for greenhouse gases. They are recognized as significant sources of N₂O, primarily due to the oxygen minimum zone (OMZ) that favors subsurface production (Gutknecht et al., 2013; Resplandy et al., 2024). Regarding CO₂, while cold surface waters enhance gas solubility, the vigorous upwelling of deep waters rich in Dissolved Inorganic Carbon (DIC) generally dominates this thermal effect, driving net CO₂ outgassing near the coast (Resplandy et al., 2024).

Beyond these EBUS, recent studies (Bachèlery, 2016; Kopte, 2017; Awo et al., 2022) have shown that the variability of Sea Surface Temperature (SST, a key upwelling indicator) at the eastern boundary of the South Atlantic was not only impacted by local wind forcing, but also by remote forcing initiated by the equatorial dynamics. Indeed, the equatorial Kelvin waves (EKW) propagating along the equator and later poleward along the coast as coastal trapped waves (CTW) have been shown to lead to the establishment of seasonal upwelling systems.

This is the case for the Gabon-Congo and Angolan tropical upwelling systems, located in the south-east of the Gulf of Guinea (GG), which are highly productive marine ecosystems (Ostrowski et al., 2009). Fishing provides around 25 % of the Angolan population's total animal protein intake and is essential for economic security (Hutchings et al., 2009; Soman and Cardoso, 2010; FAO, 2022). The seasonal variability of SST along the Angolan coast has shown an evolution that was similar to that observed in the Congo (Bachèlery et al., 2015; Bachèlery, 2016; Kopte, 2017; Awo et al., 2022; Brandt et al., 2023). It is characterized by a semi-annual pattern with an initial warming in February–April followed by a first upwelling-induced cooling in May–August. Then there is a second warming, less significant than the first, in September–November, followed by a second, less significant cooling in December–January. Following to Radenac et al. (2020) and Brandt et al. (2023), in the tropical Atlantic ocean, the thermocline and nitracline were often found at the same depth, which meant that an upward movement of the thermocline was associated with upward advection of nitrate, fueling biological productivity. Brandt et al. (2023) also

pointed out that in the Angolan tropical upwelling system, the seasonal cycle of nitrate was in phase with that of CHL_a derived from ocean color satellites (Fig. 1). Given that the wind stress along the coast was low for most of the year and out of phase with the upwelling period, the upwelling was rather shown to be induced by the passage of waves trapped at the coast, which signature was visible on the seasonal cycle of the sea level anomaly (Bachèlery, 2016; Awo et al., 2022; Brandt et al., 2023).

The cross-shore extension of the zone covered by upwelling is modulated by the regional ocean circulation (Fig. 1), dominated by the southward coastal Angola Current and Congo-Gabonese Undercurrent (Kopte, 2017; Bachèlery, 2016; Awo et al., 2022). Bachèlery (2016), based on a coupled physical-biogeochemical model, showed that equatorial remote forcing is dominant for the interannual variability of nutrients and primary production, whereas the local wind stress forcing is dominant for the sub-seasonal variability. Some studies also highlighted the important role played by turbulent mixing, locally enhanced in shallow waters near the coast (Körner et al., 2023, 2024; Tchikalanga et al., 2018; Rouault, 2012), in the seasonal modulation of SST and nutrients in Angolan coastal waters.

The Gabon-Congo upwelling zone (from 0° N to 6° S) is poorly documented. In a recent study using a high resolution (1/36°) simulation of the NEMO model over the GG, Ngakala et al. (2025) assessed the seasonal mixed layer heat budget in the Congolese upwelling system. They found that the mixed layer heat budget in the Congolese coastal area was driven by two major processes: warming by heat fluxes, dominated all year long by the solar flux, and cooling by vertical mixing at the base of the mixed layer, whereas the total advection contribution is less important, it plays a secondary role in the mixed layer heat budget. However, below the mixed layer, vertical advection by upwelling CTWs was crucial to raise the thermocline high enough so that cool waters can penetrate in the mixed layer by vertical mixing. They also mentioned that the relative contribution of vertical advection and diffusion in the mixed layer heat budget was sensitive to the criterion used to define the mixed layer.

These results were in agreement with the conclusion of Körner et al. (2023) in the northern Angolan upwelling south of the Congo River mouth. This latter study found that the net surface heat flux warmed the coastal water further, whereas turbulent mixing across the base of the mixed layer was an important cooling term. Also, Scannell and McPhaden (2018), using data from a PIRATA mooring located off the Congo River at [8° E; 6° S], found that the seasonal evolution of mixed layer properties had two main phases: a warm fresh phase (December–April) when solar heating was very efficient in warming SST in a thin mixed layer, and a cold-salty phase (May–September) driven by the intensification of southeasterly trades in response to the onset of the West African Monsoon and northward displacement of the ITCZ.

They also pointed out the necessity to take into account precipitation influence in the mixed layer heat budget.

Little information has been available at the seasonal scale for biogeochemistry in the GG. In the equatorial upwelling system, the respective contributions of physical and biological processes on the seasonality of nitrate and biological productivity, in the mixed layer and euphotic layer, have been quantified by Radenac et al. (2020). Along the coast, most studies of biogeochemical dynamics have been either limited to the section between 6° S and the Angola Benguela frontal zone (Brandt et al., 2023), or have focused on the interannual variability of biogeochemical tracers (Bachelery, 2016). The seasonal variability of biogeochemical tracers and biological productivity between 0° N and 6° S is likely influenced by three major processes: coastal upwelling, input of nutrients by the Congo River discharge (which is the second largest river discharge in the world; Hopkins et al., 2013), and the stratification linked to the Congo River freshwater. The aim of this paper is to investigate the respective roles of physical and biological processes in the seasonal cycle of nitrate and CHL_a concentration, and the respective contributions of coastal upwelling and Congo River discharge to the biological productivity in the Gabon-Congo upwelling system. The paper is organized as follows: Sect. 2 describes the numerical model and datasets; Sect. 3 presents the model validation and the nitrate budget analysis; Sect. 4 discusses the physical-biological interactions, and Sect. 5 provides the conclusions.

2 Data and methods

2.1 Numerical model

To understand the dynamics in the Gabon-Congo upwelling system, we have used the NEMO (Nucleus for European Modelling of the Ocean) ocean general circulation model based on the primitive equations discretized on an Arakawa-C grid (Madec and the NEMO System Team, 2024). The vertical mixing is computed from a turbulent closure scheme using the GLS (Generic Length Scale) formulation.

In this work, the NEMO model was coupled with PISCES (Pelagic Interactions Scheme for Carbon and Ecosystem Studies), a biogeochemical model developed by Aumont et al. (1998) and subsequently improved. Here, the version used is PISCES-2 (Aumont et al., 2015). This model has three main compartments: the first represents nutrients, including nitrogen compounds (nitrate and ammonium), iron, phosphate and silicates; the second represents phytoplankton and includes two classes, nano-phytoplankton and diatoms; the third compartment represents zooplankton, made up of two classes, microzooplankton and meso-zooplankton. We used the PISCES (cell quotas) model with constant Redfield ratios (Aumont and Bopp, 2006; Aumont et al., 2015).

A regional configuration of the GG (11° S–6° N; 10° W–14° E) with an horizontal resolution of 1/36° and 50 verti-

cal levels is used. The atmospheric forcing is derived from the JRA-55 reanalysis of the Japanese meteorological agency (Kobayashi et al., 2015), except for the wind forcing which is based on daily ASCAT (Advanced SCATterometer) satellite data at 1/4° spatial resolution. Lateral boundaries conditions are from Mercator GLORYS12V1 reanalysis data at 1/12° spatial resolution for physics and NEMO-PISCES reanalysis at 1/4° of Radenac et al. (2020) for biogeochemistry. Continental freshwater inputs for this configuration are derived from the ISBA-CTRIIP model, and in situ data from the HYBAM network for the Congo River. The NEMO configuration, ran over the period 2007–2017 (after a two-year spin-up), was validated by Ngakala et al. (2025) in our region of study. This simulation has also been validated and used in the Northern Gulf of Guinea for the coastal upwelling in summer and its interaction with mesoscale dynamics (Thiam et al., 2024). The reference simulation of the coupled biogeochemical physical model (NEMO-PISCES) was produced over the period 2007–2011, with a spin-up of 4 years for the biogeochemical part (2007–2010). We analysed monthly and daily outputs for the year 2011, which is characterised by neutral conditions regarding the Atlantic Niño and Benguela Niño interannual variability (Brandt et al., 2023).

2.2 Satellite and in-situ data

Several observational products were used to assess the model's ability to reproduce the physical and biogeochemical characteristics of the area for the year 2011. We used the MUR product (Multi-scale Ultra-high Resolution; Chin et al., 2017) with 1/4° spatial resolution and daily temporal resolution to assess the regional distribution and the seasonal cycle of SST. The vertical temperature distribution was assessed using the World Ocean Atlas (WOA; Locarnini et al., 2018; Zweng et al., 2019) climatology. The CHL_a data used came from the Globcolour product distributed by Copernicus Marine Environment Monitoring Service (<http://marine.copernicus.eu/>, last access: 11 April 2023), which combines data from four ocean color satellites, with very high spatial resolution (1 km) and daily temporal resolution.

The nutrient fields were assessed using the CSIRO Atlas of Regional Seas climatology (Ridgway et al., 2002) which merges several in situ databases (Argo buoys, WOD2005, WOCE3, Global Hydrographic Program, CTD and CMAR4 hydrology archives, NIWA5 hydrographic data, and CRC6 hydrographic data). It provides physical variables (Temperature, Salinity) and biogeochemical variables (NO₃, PO₄, O₂, Si) both at the surface and at depth with a horizontal resolution of 1/2°, 79 vertical levels from the surface to 5500 m depth, with a step of 5 m near the surface then increasing with depth, and a daily temporal resolution. This product was built from 2009 and contains data from 1940 until 2011 which was the date when the last revision of the product was made. Near surface currents from the Ocean Surface Current Analysis Real-time (OSCAR, Johnson et al., 2007) dataset

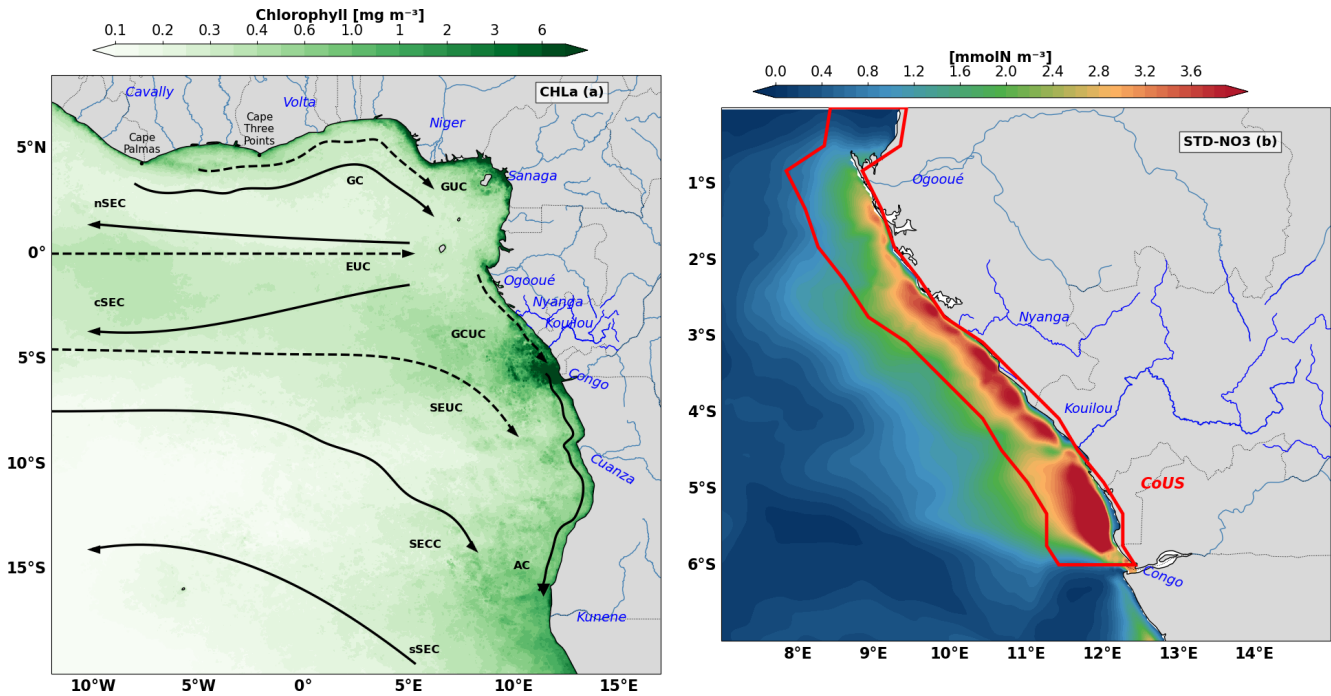


Figure 1. Regional ocean circulation and spatial distribution of biological and nutrient tracers. **(a)** Annual mean surface Chlorophyll *a* concentration (CHLa, [mg m⁻³]). The map illustrates the spatial distribution of biological productivity across the Gulf of Guinea and the South Atlantic African margin. Black arrows and dashed lines indicate the major surface and subsurface currents: northern, central and southern branches of the South Equatorial Current (nSEC, cSEC and sSEC, respectively), Equatorial Undercurrent (EUC), Guinea Current (GC), Guinea Undercurrent (GUC), Gabon-Congo Undercurrent (GCUC), South Equatorial Undercurrent (SEUC), South Equatorial Counter Current (SECC), and Angola Current (AC). **(b)** Standard deviation of Nitrate concentration (SD-NO₃, [mmolN m⁻³]). The color scale represents the variability of nitrates in the upper ocean. The red polygon delimits the coastal domain defined as the Gabon-Congo Upwelling System (CoUS), extending from the Congo River mouth (~6° S) to the Equator (~0° S), which serves as the primary study area for the nutrient budget analysis. Blue labels highlight the discharge points of the Ogooué, Nyanga, Kouilou, and Congo rivers.

are based on satellite and in situ measurements of sea surface height surface vector wind and SST. They are derived from quasi-linear and steady flow momentum equations thus combine geostrophic, Ekman and Stommel shear dynamics. OSCAR product is available on a 1/3° × 1/3° grid with a 5 d temporal resolution for year 2011, and we use it to validate the near surface currents (first 30 m) of the model outputs. Sea Level Anomaly was computed from the salto/duacs gridded product of Absolute Dynamic Topography for 2011. This product is based on sea surface height measurement of multi-mission altimeters since 1992, optimally interpolated onto 0.25° × 0.25° longitude/latitude grid (Ducet et al., 2000).

2.3 Methods

The variability of nutrients and in particular nitrate is driven by several physical and biogeochemical processes taken into account in our model. As in Radenac et al. (2020), the nitrate budget integrated over the mixed layer depth is represented by the following equation:

$$\frac{\partial \langle \text{NO}_3 \rangle}{\partial t} = - \left\langle u \frac{\partial \text{NO}_3}{\partial x} \right\rangle - \left\langle v \frac{\partial \text{NO}_3}{\partial y} \right\rangle - \left\langle w \frac{\partial \text{NO}_3}{\partial z} \right\rangle + \frac{1}{h} \left(K_z \frac{\partial \text{NO}_3}{\partial z} \right)_{z=-h} - \frac{1}{h} \frac{\partial h}{\partial t} (\langle \text{NO}_3 \rangle - \text{NO}_{3z=-h}) + \langle \text{SMS}(\text{NO}_3) \rangle \quad (1)$$

In Eq. (1), the term on the left represents the total nitrate tendency, where the brackets (...) denote the vertical average within the mixed layer of depth *h*. This depth *h* is defined as the level where the potential density exceeds the reference density at 3 m by approximately 0.06 kg m⁻³ (Aroucha et al., 2025). On the right side of the equation, the first three terms represent the zonal, meridional, and vertical advectations of nitrate, respectively, with *u*, *v* and *w* being the components of the velocity field. The fourth term represents the vertical diffusion (mixing) at the base of the mixed layer (*z* = -*h*), where *K_z* is the vertical diffusion coefficient that varies in space and time. The fifth term corresponds to the entrainment term, which represents the flux of nitrate into the mixed layer during its deepening. However, it is not explicitly solved in

our budget analysis. Following Radenac et al. (2020) for the tropical Atlantic using a similar NEMO-PISCES configuration, this term is negligible compared to other terms in the budget. Finally, the SMS (Source Minus Sink) term represents the contribution of biological processes to the spatial and temporal variability of NO_3 concentrations, as detailed in the following expression:

$$\begin{aligned} \text{SMS}(\text{NO}_3) = & \text{Nitrif} - \mu_{\text{NO}_3}^{\text{P}} \cdot P - \mu_{\text{NO}_3}^{\text{D}} \cdot D \\ & - R_{\text{NH}_4} \cdot \lambda_{\text{NH}_4} \cdot \Delta(\text{O}_2) \cdot \text{NH}_4 - R_{\text{NO}_3} \cdot \text{Denit} \end{aligned} \quad (2)$$

where Nitrif corresponds to nitrification, which is the conversion of ammonium into nitrate by bacterial activity. It is parameterized by:

$$\text{Nitrif} = \lambda_{\text{NH}_4} - \frac{\text{NH}_4}{1 + \langle \text{PAR} \rangle} (1 - \Delta(\text{O}_2)) \quad (3)$$

where NH_4 is the ammonium concentration, $\langle \text{PAR} \rangle$ is the average fraction of solar radiation available for photosynthesis, λ_{NH_4} is the nitrification rate and $\Delta(\text{O}_2)$ is the oxygen variation in the mixed layer, which provides information on the oxic and anoxic conditions of the water column: The second and third terms on the right of Eq. (2) are the growth of nanophytoplankton and diatoms, where $\mu_{\text{NO}_3}^{\text{P}}$ and $\mu_{\text{NO}_3}^{\text{D}}$ are their growth rates, P and D are their concentrations respectively. R_{NH_4} and R_{NO_3} are the stoichiometric N/C ratios of ammonification and nitrification respectively. Denit represents denitrification which occurs when the water becomes anoxic, and so nitrate (instead of oxygen) is consumed by remineralization of organic matter. A detailed description by the terms of these equations is given by Aumont et al. (2015). We used the parameter PISCES values modified for the Tropical Atlantic ocean from Radenac et al. (2020). The balance terms in Eq. (1) have been calculated online for 2011. As the lateral diffusion term is generally negligible compared with the others, it will not be discussed further.

Since the advection in Eq. (1) depends on both nitrate gradients and velocities, we investigate which component primarily controls its contribution. First, we analyze the seasonal evolution of gradient and velocity following Awo et al. (2022). Second, we evaluate the individual contributions of seasonal variations in velocity and gradient, as well as their combined effect, following Topé et al. (2023), according to Eq. (4).

$$\begin{aligned} (V_i \cdot \nabla_i(\text{NO}_3))' = & V_i' \cdot \overline{\nabla_i(\text{NO}_3)} + \overline{V_i} \cdot \nabla_i(\text{NO}_3)' \\ & + V_i' \cdot \nabla_i(\text{NO}_3)' \end{aligned} \quad (4)$$

The total seasonal variation of the advection term is thus decomposed into three distinct contributions:

$V' \cdot \overline{\nabla(\text{NO}_3)}$ (Current variability), this term quantifies the impact of current velocity anomalies acting upon a mean (steady-state) nitrate distribution. It isolates the effect of current acceleration or intensification (such as the SEUC or the

Angola Current) on nutrient transport. $\overline{V} \cdot \nabla(\text{NO}_3)'$ (Gradient variability), this term represents the impact of seasonal changes in the nitrate concentration gradient under a mean circulation. It highlights the influence of seasonal water mass enrichment, particularly via the Congo River plume. $V' \cdot \nabla(\text{NO}_3)'$ (Non-linear term), this term accounts for the simultaneous interaction between current fluctuations and gradient fluctuations. To determine which of these mechanisms predominantly governs the nitrate budget, Pearson correlation coefficients were calculated between the total advective anomaly and each decomposed component. This statistical approach serves a critical physical objective: it allows us to disentangle whether the seasonal nitrate supply is driven primarily by the kinematic modulation of the flow (circulation-driven) or by the pulsing of the nutrient source (supply-driven). A high correlation with the current term would identify regional circulation such as the SEUC or Angola Current as the primary pump, whereas a dominant correlation with the gradient term would pinpoint the massive periodic enrichment, particularly from the Congo River plume, as the main trigger of nitrate variability. All reported correlations are statistically significant at a 95 % confidence level ($p < 0.05$). By establishing this statistical hierarchy, we can physically characterize the system as being either transport-limited or supply-limited, providing a rigorous diagnostic of the processes regulating primary productivity in the Gabon-Congo upwelling. The Primary production (NPP) was calculated from the phytoplankton evolution equation (Aumont et al., 2015):

$$\text{NPP} = (1 - \delta^{\text{P}}) \mu^{\text{P}} \cdot P \quad (5)$$

In this equation, P is the phytoplankton biomass (diatoms), δ^{P} represents the exudation of the phytoplankton (diatoms). μ^{P} is the specific growth rate of the phytoplankton taking into account nutrient and light availability. Note that this equation applies to each phytoplankton species (diatoms or nanophytoplankton), and total NPP is the sum of NPP from both diatoms and nanophytoplankton. μ^{P} is the specific growth rate of the phytoplankton taking into account nutrient and light availability.

NPP, which represents the organic matter synthesized by phytoplankton after accounting for autotrophic respiration, is calculated online by the coupled NEMO-PISCES model. Within the model framework, NPP is partitioned into New Production (NP), fueled by external nutrient inputs (primarily nitrate) through advection and diffusion, and Regenerated Production (RP), sustained by nutrients recycled within the euphotic zone (primarily ammonium). Both NP and RP components are computed online, providing a detailed breakdown of the trophic status and nutrient utilization efficiency in the Gabon-Congo upwelling system.

3 Results

3.1 Model/data comparison

3.1.1 Spatial variations during the upwelling period

The assessment of our model simulation has been done using several observation products of physical variables, including Sea Surface Temperature (SST), Sea Surface Height (SSH), and ocean currents, as well as biogeochemical tracers such as nitrate (NO_3) and CHLa, based on both satellite and in situ data. Figure 2 shows the regional distribution from observations and model outputs for both SST (Fig. 2a–b), nitrate concentration (Fig. 2c–d) and CHLa concentration (Fig. 2e–f), averaged for austral winter (June, July and August) which is the main Gabon-Congo upwelling period (Ngakala et al., 2025). As can be seen, the upwelling feature is well captured by the model with cooling of surface water at the coast below 23°C in the model and 22°C in the MUR product (Fig. 2a, b). This cooling feature is consistent with high nitrate (Fig. 2c, d) and CHLa (Fig. 2e, f) concentrations in both models and observation, particularly north of the Congo estuary (6°S) and nearby Kouilou River mouth (Fig. 2e) at 4.47°S . These cool and enriched nutrient coastal waters are spread offshore displaying a cross-shore gradient, with a greater extension in the observation than the model. The highest nitrate concentration in the coastal waters is greater than 10 mmolN m^{-3} in the model (8 mmolN m^{-3} in the observation) located mainly in the Congo River plume area, inducing enhancement of PP resulting in a strong CHLa signature.

The offshore area ($7\text{--}10^\circ\text{E}$) is the oligotrophic zone characterized by relatively warm waters (24.5°C in the model and 23.5°C in the observation), depleted in nitrate and less productive in CHLa concentration. In this offshore area nitrate concentrations are lower than 1.6 mmolN m^{-3} in the observation and 0.8 mmolN m^{-3} in the model.

Although the model captures relatively well the regional distribution of the 3 variables, we can see some differences. For instance, the model is warmer than observations by about 1°C and shows stronger nitrate concentration (by about 2 mmolN m^{-3}) and CHLa concentration ($6\text{--}10\text{ mg m}^{-3}$) at the coast. In the offshore area, the model seems to be less enriched in nitrate concentration than the observation by about 0.8 mmolN m^{-3} .

High variability of nitrate concentration is found in the coastal Gabon-Congo area (Fig. 1b) and in the Congo river plume zone as we can see in model annual standard deviation distribution of NO_3 . Therefore the red box ($0\text{--}6^\circ\text{S}$, 1° width coastal band) in Fig. 1b is used to analyze the vertical nitrate profile to assess the model's ability to capture its vertical distribution. This area corresponds to our studied area in the Gabon-Congo coastal upwelling zone.

Very close to the surface, water masses are nutrient depleted for both model and observation (Fig. 3), likely due to

photosynthesis activity of phytoplankton that consumes nitrate in presence of light, increasing its biomass thus CHLa concentrations. However this depletion is more pronounced in the model than in the observation. In the subsurface, the high nitrate concentration is due to the remineralization of organic matter by bacteria and coastal upwelling of deeper enriched nitrate waters, with the model showing higher concentrations than observed. Although nitrate isolines are shallower in the model than in observations below about 15 m depth, some nitrate isolines are relatively well captured by the model, for instance isolines 7 and 10 mmolN m^{-3} .

3.1.2 Seasonal cycle of SST, nitrate, SLA and current in the Gabon-Congo coastal area

Now we use the coastal box defined in Fig. 1b to evaluate the seasonal cycle of nitrate. The nitrate seasonal variability is characterized by a semi-annual cycle with two maxima and two minima in the model and the observations. The main maximum occurs from May to September when SST reaches its minimum of 20°C in both model and observations (Fig. 4c, d) and the secondary maximum occurs in December when SST reaches a secondary minimum of 25.5°C in the model and 24.5°C in observation. We have a warmer SST reaching 30°C from January to April and 26°C from October to November in both the model and the observations. This semi-annual SST cycle is likely due to CTWs propagation since it is consistent with the SLA seasonal cycle (minimum SST corresponds to negative SLA and maximum SST corresponds to positive SLA) as mentioned earlier by Ngakala et al. (2025) in the same area. Indeed, the propagation of CTWs induce vertical migration of the thermocline resulting thereby in cooling or warming at the surface. At the seasonal scale, the propagation of upwelling CTWs from May to September and in November–December uplifts thermocline, supplying cold waters to the surface and reducing Sea Surface Height (SSH) by steric effect. As downwelling CTWs propagate from January to April and in September–October, they deepen thermocline, warming the surface and increasing SLA. The cold waters upwelled by CTWs (May–September) are highly enriched in nitrate, whereas warm surface waters induced by downwelling CTWs (January–April and September–October) are nitrate depleted. The seasonal variability of SLA due to CTWs (Fig. 4a, b) is consistent with the seasonal variability of SST (Fig. 4c, d) and of nitrate concentration (Fig. 4e, f) in both the model and observations. The highest nitrate concentration is around 10 mmol m^{-3} near the Congo River mouth (6°S) and decreasing northward, however the observations seem to be richer in nitrate than the model. In December during the secondary cooling, nitrate concentration in the model is greater by about 1.2 mmol m^{-3} than observed along the coast. In the warming period (January–April and October–November), this coastal area seems to be nitrate depleted.

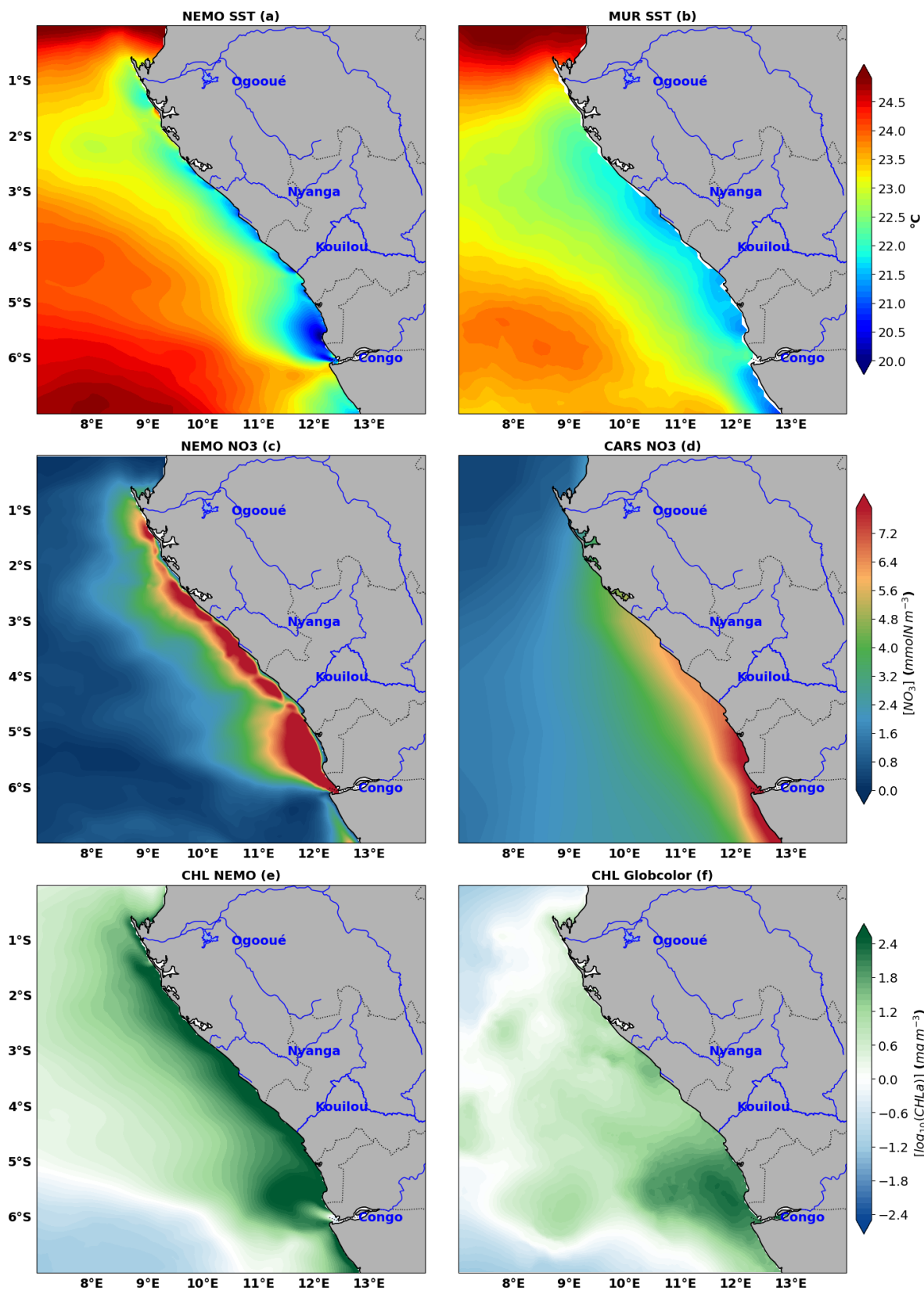


Figure 2. Comparison between model (left hand side) and observations (right hand side) with regional distribution of sea surface temperature (a, b), nitrate concentration (c, d) and CHLa concentration (e, f) averaged for austral winter (June, July, August).

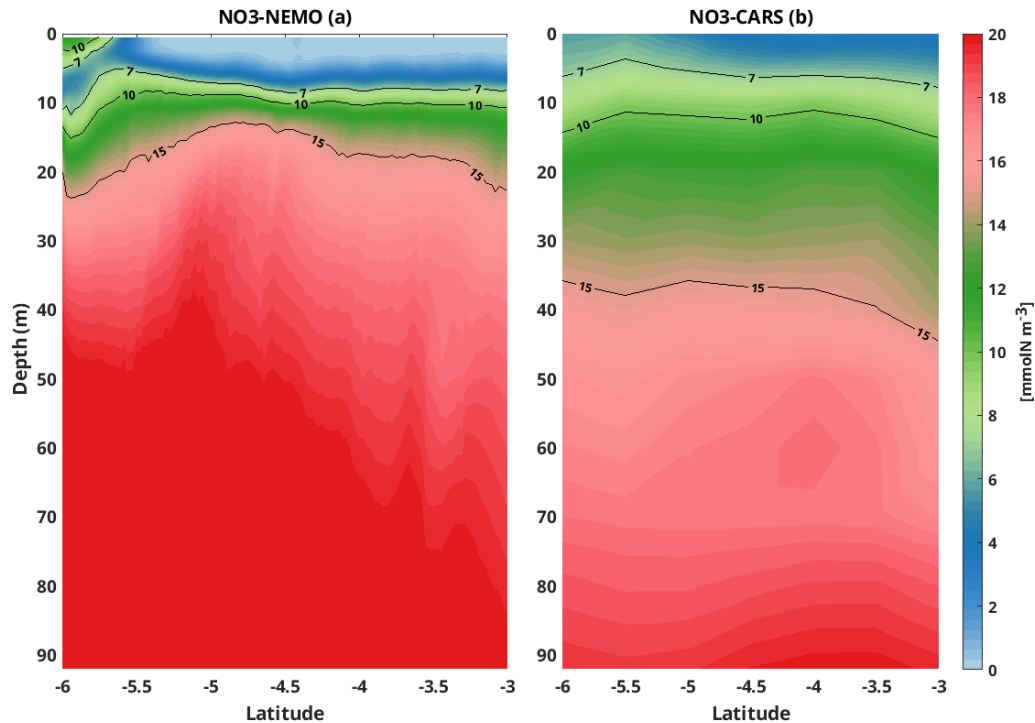


Figure 3. Comparison between model (a) and observation (b) using vertical distribution of nitrate concentration in the first 90 m, in the coastal box (3–6° S and 1° width band to the coast) in the main upwelling season (June, July and August). black represents nitrate concentration isolines.

Despite the model capturing the SLA signature, the observed seasonal cycle of SLA remains more intense than in the simulation. This feature is driven by the combined effect of remotely forced Equatorial Kelvin Waves (EKW) and poleward-propagating CTWs (Bachèlery, 2016; Kopte, 2017; Awo et al., 2023; Brandt et al., 2023). During cooling periods, upwelling CTWs decrease the SLA and uplift the thermocline. Following Radenac et al. (2020), the thermocline depth in this region acts as a reliable proxy for the nitracline; its upward migration significantly enhances nitrate supply to the surface, fueling biological productivity. Conversely, the downwelling waves observed in the warming periods increase the SLA and deepen the nitracline, leading to the nutrient-depleted conditions described previously.

High nitrate concentrations support biological production, therefore correspond to high CHLa signals at the surface (Fig. 5). On the contrary, during the warming period, the downwelling CTWs propagating along the coast increase SLA, deepen the thermocline (Ngakala et al., 2025). This also deepens the nitracline and consequently deplete the nitrate concentration at the ocean surface, thus the low CHLa signal (Fig. 5).

The variability of simulated near-surface currents between 0 to 15 m depth (Fig. 6) was compared to the OSCAR product. Here, we make a latitudinal section at 4° S and look at the seasonal cycle of meridional currents (Fig. 6a and b) from 7° E to the coast for both the model (Fig. 6a) and observations

(Fig. 6b). We do not restrict to the Gabon-Congo box as we have done for other variables, because the OSCAR product is not well resolved at the vicinity of the coast. So we can see that the model reasonably represents the seasonal variability of meridional currents with northward velocities in April, June–September and November–December with the magnitude of around 0.1 m s^{-1} . In the observations, this structure is more or less similar, but we can see some differences: southward velocities between 8.5 and 10.2° E in July, and also between 7 and 9° E during August–September and January, are not found in the model.

Nevertheless, we can see in both products southward currents in February–March and October with a strong magnitude of 0.25 m s^{-1} in the observations though only 0.15 m s^{-1} in the model. This seasonal structure is consistent with the seasonal cycle of meridional currents off Angola, further south, and the southward flow in February–March and October seems to be the Angola current (Kopte, 2017). To assess the zonal current (Fig. 6c and d), we make a longitudinal section at 10° E and we look at the seasonal cycle of zonal current between 3° S and 7° S. The modeled zonal structure with westward velocities from April to August and November–December has a magnitude of about 0.1 m s^{-1} along the section (Fig. 6c), in agreement with the observations (Fig. 6d), which also show westward velocities from April to August. However there are some differences with the model from March to August between 3 and 4.5° S where

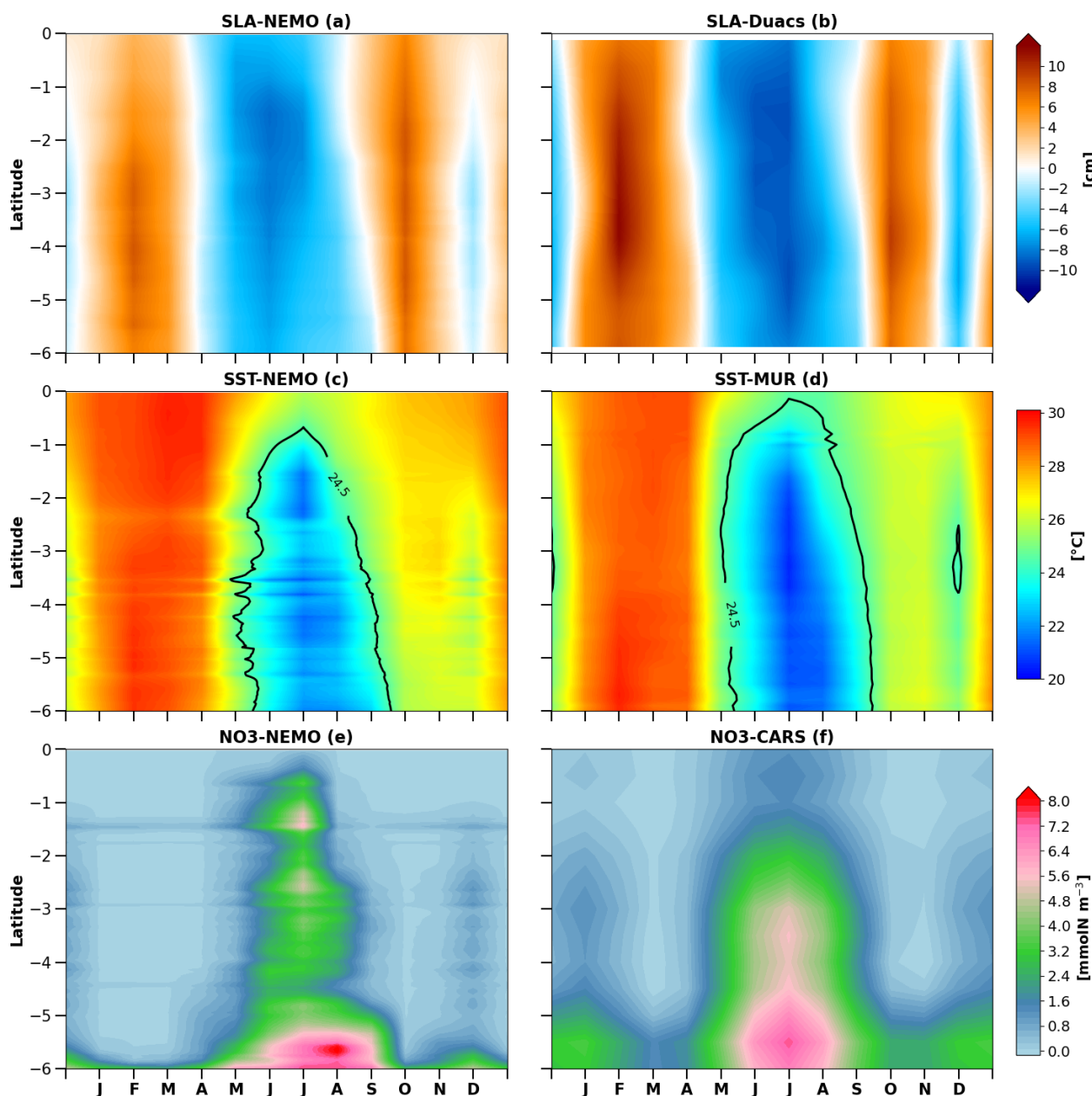


Figure 4. Comparison between modeled (left) and observed (right) seasonal cycles of Sea Level Anomaly (a, b), SST (c, d) and nitrate concentration (e, f) averaged in the coastal box (6–0° S, 1° width).

we can observe very strong (more than 0.5 m s^{-1}) eastward flow. In contrast to the model, the flow during November is eastward in the observation. The noticeable similitude is the eastward flow in January–February and October with a magnitude of 0.15 m s^{-1} which seems to be the signature of the South Equatorial UnderCurrent (SEUC). This eastward current is deeper further offshore (100 m depth) west of 0° E (Bourlès et al., 2004) and rising near the surface near the coast (Nubi et al., 2016; Assene et al., 2020).

3.2 Nitrate budget in the mixed layer

Generally, the seasonal variations in CHLa are thought to be primarily related to seasonal variations of the nitrate input in the equatorial Atlantic ocean (Loukos and Mémerly, 1999; Radenac et al., 2020) and in the tropical Angolan upwelling (Brandt et al., 2023). This is probably the case also in the Gabon-Congo coastal area, where the seasonal cycles of nitrate (Fig. 7a) and CHLa (Fig. 5) in our model are very consistent. Corresponding to the semi-annual variability of nitrate, the seasonal change rate of its concentra-

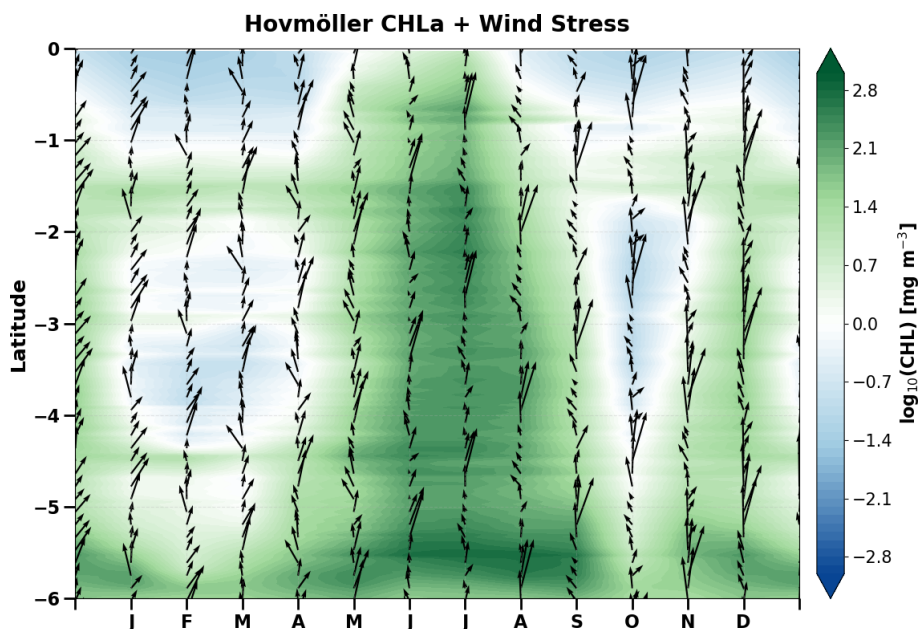


Figure 5. Seasonal cycle of CHLa concentration (in background) and wind stress (black arrow) along the Gabon-Congo coastal box (6–0° S, 1° width) area in the model.

tion (Fig. 8b) displays a four-phase cycle: a first increasing phase between March and August with a highest amplitude ($0.3 \text{ mmol m}^{-3} \text{ d}^{-1}$) in July, followed by a decreasing phase in September–November with a highest amplitude in October ($0.01 \text{ mmol m}^{-3} \text{ d}^{-1}$ north of 5° S and about -0.13 to $-0.3 \text{ mmol m}^{-3} \text{ d}^{-1}$ between 5 and 6° S all years long).

Then we have a weak second increasing phase in November–December of about $0.1 \text{ mmol m}^{-3} \text{ d}^{-1}$ and a weak decreasing phase in January–February ($0.01 \text{ mmol m}^{-3} \text{ d}^{-1}$). This semi-annual cycle is due to a balance between nitrate supply by physical processes (Fig. 7c), maximum during the main upwelling period, and nitrate consumption by biological processes (Fig. 7d).

3.2.1 Seasonal Nitrate Budget Analysis: Horizontal Vs Vertical Contributions

Looking at our previous results, we saw that physical processes drive the nitrate supply in the Gabon-Congo upwelling system, now we will look at the contribution of horizontal and vertical processes to understand which are the main drivers for this nitrate supply. Figure 8 shows that horizontal and vertical processes (Fig. 8a and b respectively) are of great importance for nitrate supply.

In fact, as we can see in the Fig. 8, vertical processes (Fig. 8b) are the main driver of nitrate supply during the upwelling between 0 and 5.5° S with an input magnitude of around $1 \text{ mmol m}^{-3} \text{ d}^{-1}$ along the coast while the horizontal processes are the main driver at the vicinity of Congo river mouth (5.5 – 6° S) all year long. The latter seems to be dominated by zonal advection (Fig. 8c) with a very high nitrate

input of more than $1.2 \text{ mmol N m}^{-3} \text{ d}^{-1}$ nearby 6° S with a northward extension, largest firstly in November–December and secondly in June–July. This is consistent with the seasonal maximum of Congo River discharge, which suggests a nitrate input through the river plume (Hopkins et al., 2013). North of 6° S , meridional advection (Fig. 8e) drives horizontal processes.

The nitrate budget analysis reveals also that vertical processes (Fig. 8b) are dominated by vertical mixing (Fig. 8f), while vertical advection has the same seasonality but a smaller contribution (Fig. 8d). Indeed, the nitrate input by the vertical diffusion is about $0.7 \text{ mmol N m}^{-3} \text{ d}^{-1}$ but only around $0.5 \text{ mmol N m}^{-3} \text{ d}^{-1}$ by vertical advection. Both vertical processes decrease nitrate concentration nearby 6° S , under Congo River plume influence with the dominant zonal advection contribution. Indeed, as nitrate concentration is greater in the near-surface Congo River plume than in subsurface (between 5 to 10 m , see Fig. 3), deeper waters rising at the surface by vertical advection reduce nitrate in the plume area.

Similarly, vertical mixing of subsurface waters with the plume waters decreases nitrate concentration at the surface, although the strong haline stratification associated with the Congo River plume limits this effect.

It is important to note that, on the one hand, vertical advection (Fig. 8d) and vertical diffusion (Fig. 8f) have the same seasonality as SLA (Fig. 4a), in opposite phase, northward of 5.5° S . This suggests that the upwelling associated with CTWs (negative SLA) induce these vertical processes and therefore drive the input of nitrate in the northern part of the

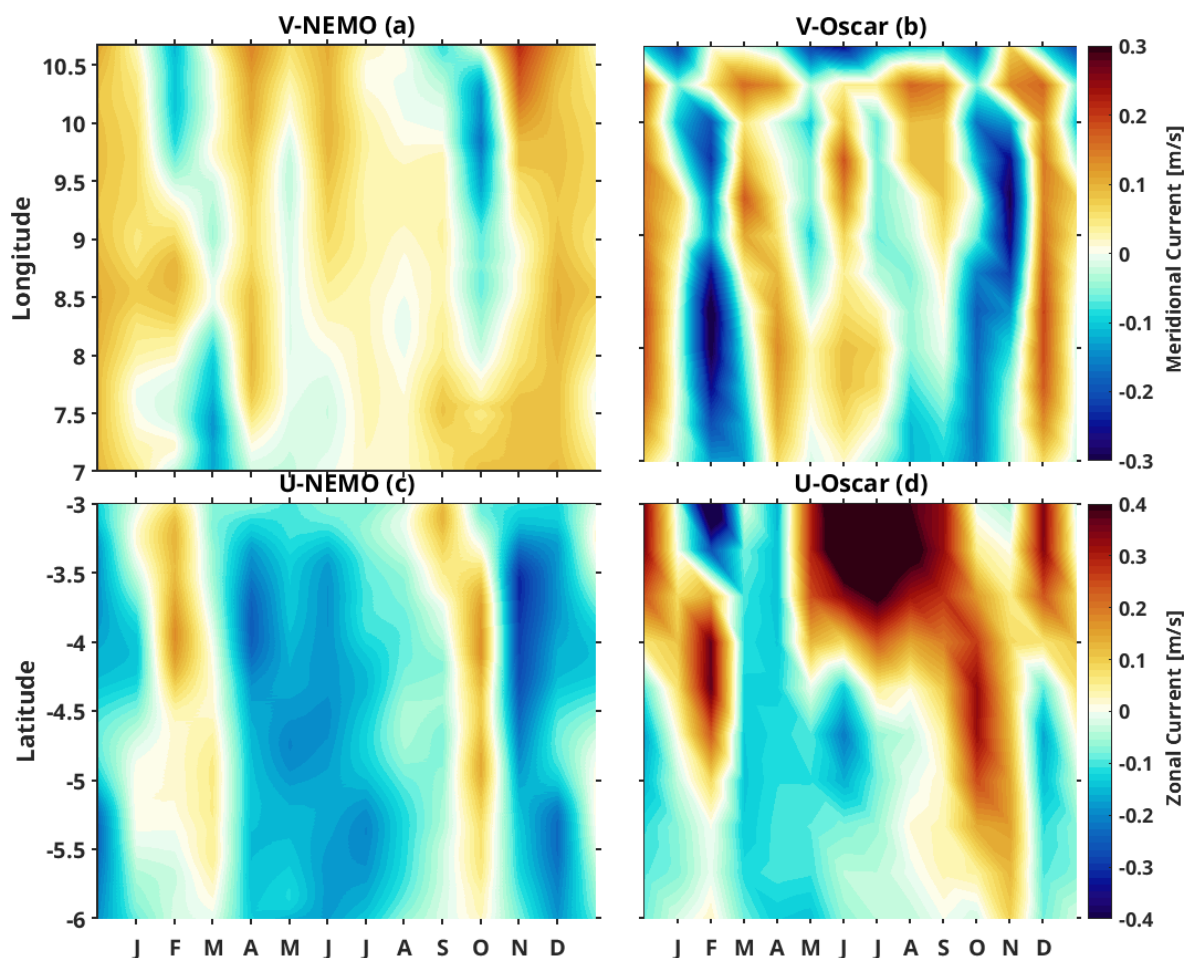


Figure 6. Seasonal cycle of surface current, zonal current (a, b) at 10° E section and between 3 and 7° S and meridional current (c, d) at 4° S section from 7° E to the coast.

Gabon-Congo coast. On the other hand, horizontal advection (both zonal and meridional advectons) has the same seasonality as the Congo River discharge between 5.5 and 6° S. This suggests that the Congo River supplies nitrate through zonal advection, near its mouth.

3.2.2 Regional Nitrate Budget Analysis in the main upwelling period: Physical Vs Biological Contributions

The regional distribution of nitrate balance terms averaged over the mixed layer for the austral winter (June–July–August), when upwelling reaches its maximum intensity, is presented in Fig. 9. The nitrate tendency (Fig. 9b) shows that during the upwelling period, nitrate input occurs throughout the domain with values varying between -0.3 to 0.3 $\text{mmolN m}^{-3} \text{d}^{-1}$ in the plume zone and 0.2 to 0.56 $\text{mmolN m}^{-3} \text{d}^{-1}$ along the coast in the northern part. In the offshore zone, the nitrate tendency is lower, with a magnitude of around 0.05 $\text{mmolN m}^{-3} \text{d}^{-1}$. This distribution of the nitrate tendency shows that the input of nitrate by

physical processes (Fig. 9c) is slightly greater than the uptake of nitrate by biological processes (Fig. 9d) throughout the area, explaining the positive nitrate change rate, except at the Congo River mouth where we have negatives values. Figure 9a shows that nitrate inputs along the coast are very high close to river mouth and varies a lot along the coast over a width of about 165 km from the coast. During this main period of upwelling, in general, vertical processes (Fig. 10b) largely dominate the nitrate supply across the entire continental shelf. A continuous coastal band of strong enrichment is observed, with values often exceeding 0.513 to 0.677 $\text{mmolN m}^{-2} \text{d}^{-1}$. Conversely, horizontal processes (Fig. 10a) show a more localized and overall lower contribution throughout the domain, with the notable exception of the Congo and Ogooué River mouth (~ 6 and 1° S respectively), where a massive positive flux (dark red, > 0.677 $\text{mmolN m}^{-2} \text{d}^{-1}$) is observed. Comparing the spatial structure of the total horizontal process (Fig. 10a) with its individual components reveals a striking similarity to zonal advection (Xad, Fig. 10c). The Xad signal

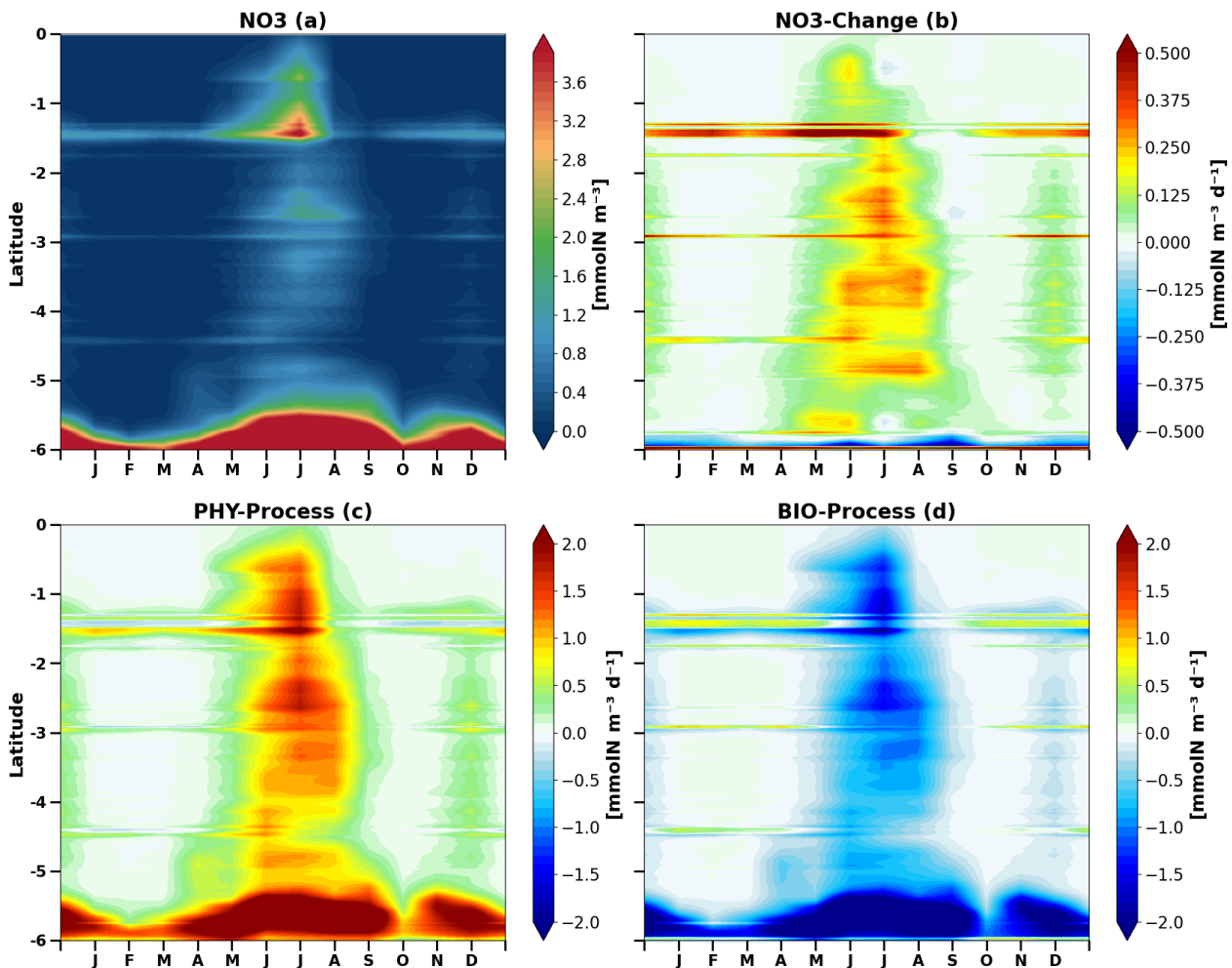


Figure 7. Latitude-time Hovmöller diagram of the model seasonal cycle of Mixed Layer Nitrate (MLN) budget (a), the rate of the MLN change (b), the physical process contribution (c) and the biological process contribution (d) along the Gabon-Congo coast. Units are mmolN m^{-3} and $\text{mmolN m}^{-3} \text{d}^{-1}$ for (a) and (b), (c), (d), respectively.

(Fig. 10c) almost perfectly reproduces the nitrate patch observed at the Congo mouth, indicating that zonal transport (east–west) is the main driver of horizontal nitrate injection into the mixed layer, associated with the offshore extension of the river plume. Although meridional advection (Yad, Fig. 10e) exhibits significant dipole structures near the Congo and patches along the coast, its intensity and spatial pattern provide a less compelling explanation for the overall horizontal process signal. It can therefore be concluded that zonal advection is the dominant term dictating the distribution of horizontal fluxes in this region. The study of vertical components shows that the total vertical process (Fig. 10b) results from two distinct yet complementary mechanisms. Vertical advection (Zad, Fig. 10d) shows very intense ($> 0.677 \text{ mmolN m}^{-2} \text{d}^{-1}$) but highly localized supply along the coastline and capes, representing the typical signature of coastal upwelling driven by wind and Coastally Trapped Waves (CTWs). However, vertical diffusion (Zdf,

Fig. 10f) shows the strongest resemblance to the overall Vert_Process. It exhibits a broad and homogeneous distribution extending well offshore from the coast, with sustained values between 0.349 and $0.513 \text{ mmolN m}^{-2} \text{d}^{-1}$. Unlike advection, which is highly segmented, vertical diffusion better explains the spatial continuity of nitrate supply across the shelf. This suggests that while advection (upwelling) brings nitrate to the base of the mixed layer, turbulent mixing (diffusion) ensures its effective distribution toward the surface across the entire domain.

3.3 Nitrate budget in the euphotic layer and along the water column

Now, in addition to the processes acting in the surface mixed layer, we investigate other processes involved in the nitrate budget below the mixed layer by analysing the nitrate budget in the euphotic layer, generally defined as the zone where light penetration exceeds 1% of the surface light, allowing

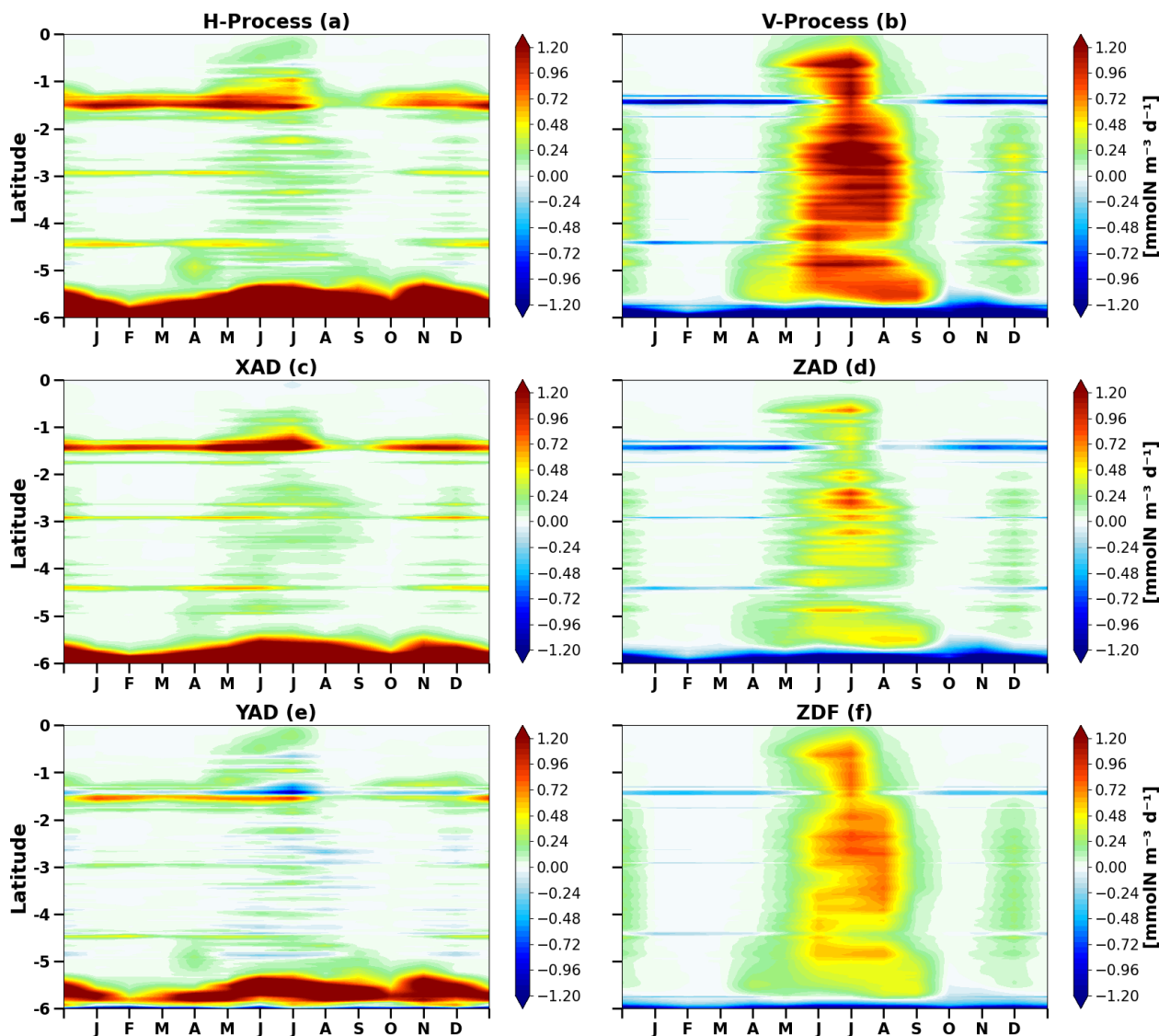


Figure 8. Latitude-time Hovmöller diagram of the model seasonal cycle of horizontal (a) and vertical (b) process contributions, zonal (c), meridional (e), vertical (d) advectons, vertical diffusion (f) averaged in the mixed layer along the Gabon-Congo coast. Units are $\text{mmolN m}^{-3} \text{d}^{-1}$.

for the presence of phytoplankton and other photosynthetic organisms. The seasonal variations of thermocline, mixed layer and euphotic layer depths are compared in Fig. 11. In Fig. 11a, the thermocline (20°C isotherm) variation is very close to the nitracline as suggested by Radenac et al. (2020). The mixed layer euphotic layer is very shallow (~ 10 m) throughout the year probably due to the Congo River plume stratification. The euphotic layer extends deeper than the mixed layer, but is generally shallower than the thermocline, except from June to September. The euphotic layer gets thinner during upwelling through the enhancement of CHLa concentration which reduces light penetration (self-shadowing by CHLa). Overall the nitrate tendency (Fig. 11b) has the same semi-annual variation in the euphotic layer than in the

mixed layer, although more intense in the euphotic layer with a maximum at the bottom of the euphotic layer. In fact, most nitrate input by physical processes (Fig. 11c) happens in the mixed layer, where it is almost balanced by biological nitrate uptake (Fig. 11d). In contrast, in the euphotic layer below the mixed layer (between 10 and 40 m depth), biological processes are poorly active and the nitrate variability is almost exclusively induced by physical processes. The mean nitrate input in the euphotic layer is about $0.1 \text{ mmolN m}^{-3} \text{d}^{-1}$ during the main upwelling period and the maximum input ($0.2 \text{ mmolN m}^{-3} \text{d}^{-1}$) occurs in May at the base of the euphotic layer (Fig. 11b).

In the euphotic layer, biological activity is dominated by photosynthesis which removes nitrate, whereas below the

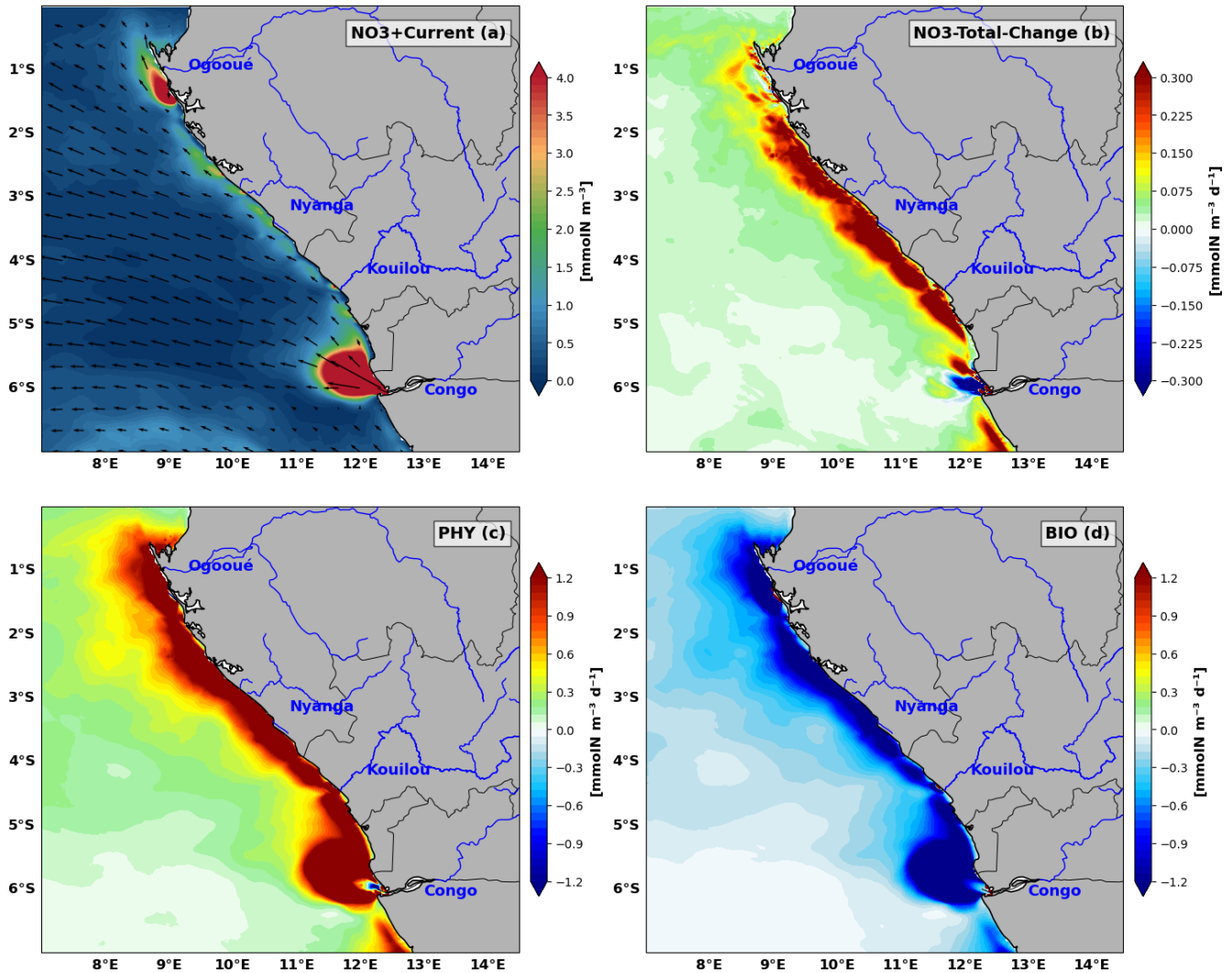


Figure 9. Spatial distribution averaged over the main upwelling period of (a) nitrate, (b) nitrate tendency contributed by (c) physical processes and (d) biological processes, all averaged in the mixed layer in Austral winter. The mean current in the mixed layer is superimposed in (a). Nitrate concentration units are mmolN m^{-3} and the tendency terms units are $\text{mmolN m}^{-3} \text{d}^{-1}$.

euphotic layer remineralization supplies nitrate with about $0.05 \text{ mmolN m}^{-3} \text{d}^{-1}$ almost all year long (Fig. 11d).

3.3.1 Euphotic Layer Nitrate Budget Analysis: Horizontal Vs Vertical Contributions

Figure 12 shows that, even in the euphotic layer, the physical contribution to nitrate supply (Fig. 11c) is mostly driven by vertical processes (Fig. 12b). However, the large decrease in nitrate (Fig. 11b) in October is also caused by horizontal contributions (Fig. 12a) in the euphotic layer. Between the surface and 5 m depth, horizontal processes dominate nitrate input (Fig. 12e). In the euphotic layer below, meridional advection is the main driver of nitrate removal almost year-round, particularly in June and October.

Zonal advection (Fig. 12c) supplies nitrate in the euphotic layer, with a maximum above the mixed layer depth, throughout the year. This nitrate input is more than compensated by nitrate lost by meridional contribution, below the upper 5 m (Fig. 12e), except in June, July and August. Vertical advection (Fig. 12d) is the dominant vertical process (Fig. 12b) in the nitrate budget. Below 30 m depth, it has a semi-annual cycle characteristic of upwelling and downwelling CTWs propagation, associated with nitrate increase when the thermocline shallows and nitrate decrease when the thermocline deepens, with the maximum and minimum values around the thermocline depth. Moreover, vertical advection supplies more nitrate in the mixed layer than in the euphotic layer below during the main upwelling period (June, July and August), but rather the opposite during the second upwelling period (December). Between the mixed layer depth and the

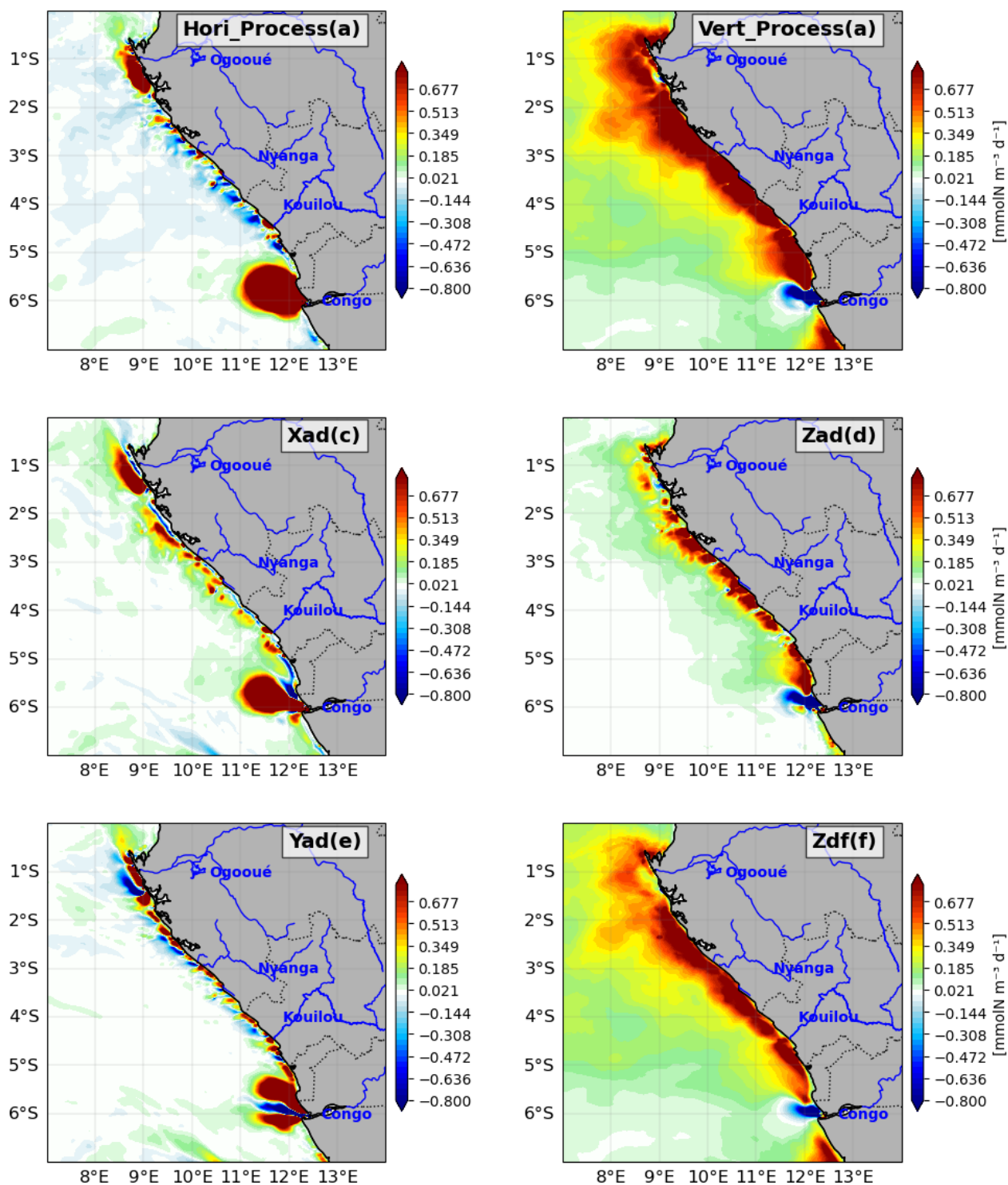


Figure 10. Contribution of (a) the horizontal processes, including (c) zonal advection and (e) meridional advection, and (b) vertical processes, including (d) vertical advection and (f) vertical diffusion, to the nitrate budget averaged in the mixed layer during the austral winter. Units are $\text{mmolN m}^{-3} \text{d}^{-1}$.

euphotic layer depth, vertical diffusion (Fig. 12f) tends to partially compensate for the effects of vertical advection on nitrate. However, in the mixed layer it mostly supplies nitrate, particularly during the upwelling seasons.

3.3.2 Nitrate budget analysis: advection components analysis

As nitrate advection depends on velocity and on the nitrate gradient, we now evaluate the individual contributions of seasonal variations in velocity and nitrate gradient, as well as their combined effect, to the seasonal variations of nitrate advection (see Sect. 2.3, Eq. 4).

Horizontal advection

Figure 13 allows to visually compare the depth-time structure of the zonal nitrate advection (Fig. 13a) with that of its different components, while correlation r is used to quantify the comparison.

The seasonal cycle of zonal nitrate advection in the 0–100 m water column (Fig. 13a) is controlled first by the term $\bar{u} \cdot \nabla_x(\text{NO}_3)'$ (Fig. 13e, $r = 0.77$, $p < 0.05$), i.e. the annual mean zonal current multiplied by the seasonal variations of the nitrate zonal gradient, second by the term $u' \cdot \nabla_x(\text{NO}_3)$ (Fig. 13d, $r = 0.49$, $p < 0.05$), i.e. the seasonal variations of the zonal current multiplied by the annual mean nitrate zonal gradient, and third (and much less) by the term. The third component, which represents the simultaneous variation in zonal current and nitrate gradient $u' \cdot \nabla_x(\text{NO}_3)'$, (Fig. 13f, $r = -0.15$, $p < 0.05$), i.e. the product of seasonal variations of both the zonal current and the nitrate zonal gradient. The seasonality of the zonal current (Fig. 13c) is influenced by the seasonal cycle of the South Equatorial Undercurrent (SEUC), with maximum values in September–October and February–March (Siegfried et al., 2019) in this zone (0–6° S, 1° from the coast). Thus we can conclude that the SEUC plays a key role in the nitrate balance in the Gabon-Congo system by bringing nitrate in February–March and in September–October to the euphotic layer.

In the euphotic layer, we see that, as for the meridional nitrate advection, the meridional current (Fig. 14c) looking at the shape seems to be the main factor in the vertical and temporal variation shape of the meridional nitrate advection (Fig. 14a). The Angola current (AC), is the factor which modulates nitrate lost by meridional nitrate advection throughout the year, with maximum loss in September–October and June–July, in and below the euphotic layer, except in the first 5 m-depth.

Our analysis in this section reveals that the simultaneous variation in both the meridional current and the gradient ($v' \cdot \nabla_y(\text{NO}_3)'$, Fig. 14f) exhibits the highest correlation ($r = 0.527$, $p < 0.05$) with meridional nitrate advection, thus explaining the major changes in advection. This result highlights the significant impact of the concurrent variability of

both meridional current and gradient on meridional nitrate advection in the euphotic layer. In contrast, gradient variation ($\bar{v} \cdot \nabla_y(\text{NO}_3)'$, Fig. 14e) is poorly correlated ($r = 0.97$, $p < 0.05$) with meridional nitrate advection. The very low positive correlation with total meridional advection (a) indicates this term, representing the effect of a mean meridional current acting on a fluctuating nitrate gradient. This suggests that either the mean meridional current is weak, or its interaction with the fluctuating gradient does not lead to significant changes in overall advection. The variation in the meridional current ($v' \cdot \nabla_y(\text{NO}_3)$, Fig. 14d) shows the lowest correlation ($r = 0.287$, $p < 0.05$). This low, negative correlation with total meridional advection (Fig. 14a) indicates that this term, representing the effect of fluctuating meridional currents on a relatively stable mean nitrate gradient, is not a dominant driver of the overall meridional nitrate advection. In fact, a negative correlation suggests it might weakly oppose the main advection pattern or have an inverse relationship. This implies that the mean gradient is either small or the meridional current variations are not aligned to produce significant advection changes via this mechanism.

Vertical processes

Our analysis reveals that within the euphotic layer, the variation in the vertical gradient $\bar{w} \cdot \nabla_z(\text{NO}_3)'$, Fig. 15e) appears to better explain the variation in vertical nitrate advection (Fig. 15a), showing a correlation of $r = 0.79$ ($p < 0.05$). In contrast, vertical velocity variation ($w' \cdot \nabla_z(\text{NO}_3)$, Fig. 15d) plays a secondary role, with a correlation of approximately 0.646 ($p < 0.05$) with vertical nitrate advection. Looking now at the vertical nitrate advection, we can see strong similarities in the vertical and temporal variation structure between vertical advection seasonality (Fig. 15a), vertical nitrate gradient seasonality (Fig. 15b) and vertical velocity seasonality (Fig. 15c), both three are very strong in the euphotic layer. We can also see in the semi-annual vertical velocity that from April to August and November–December, vertical velocities are upward corresponding to negative values of SLA (Fig. 4a, b), lowest SST (Fig. 4c, d) values and highest nitrate concentration (Fig. 4e, f). From January to March and September–October, vertical velocities are downward corresponding to positive values of SLA (Fig. 4a, b), highest SST (Fig. 4c, d) values and lowest nitrate concentration (Fig. 4e, f). This later observation confirms that CTWs propagating from April to August and November–December are associated with upwelling. In contrast, CTWs propagating from January to March and September–October are associated with downwelling. Note that similar results were found by Ngakala et al. (2025) for the seasonal heat budget in the Gabon-Congo upwelling (from 4–6° S and 1° width to the coast) and also further south in the Angolan upwelling by Körner et al. (2024).

However, if we average in the first hundred meters, vertical velocity variation has the highest correlation of 0.831

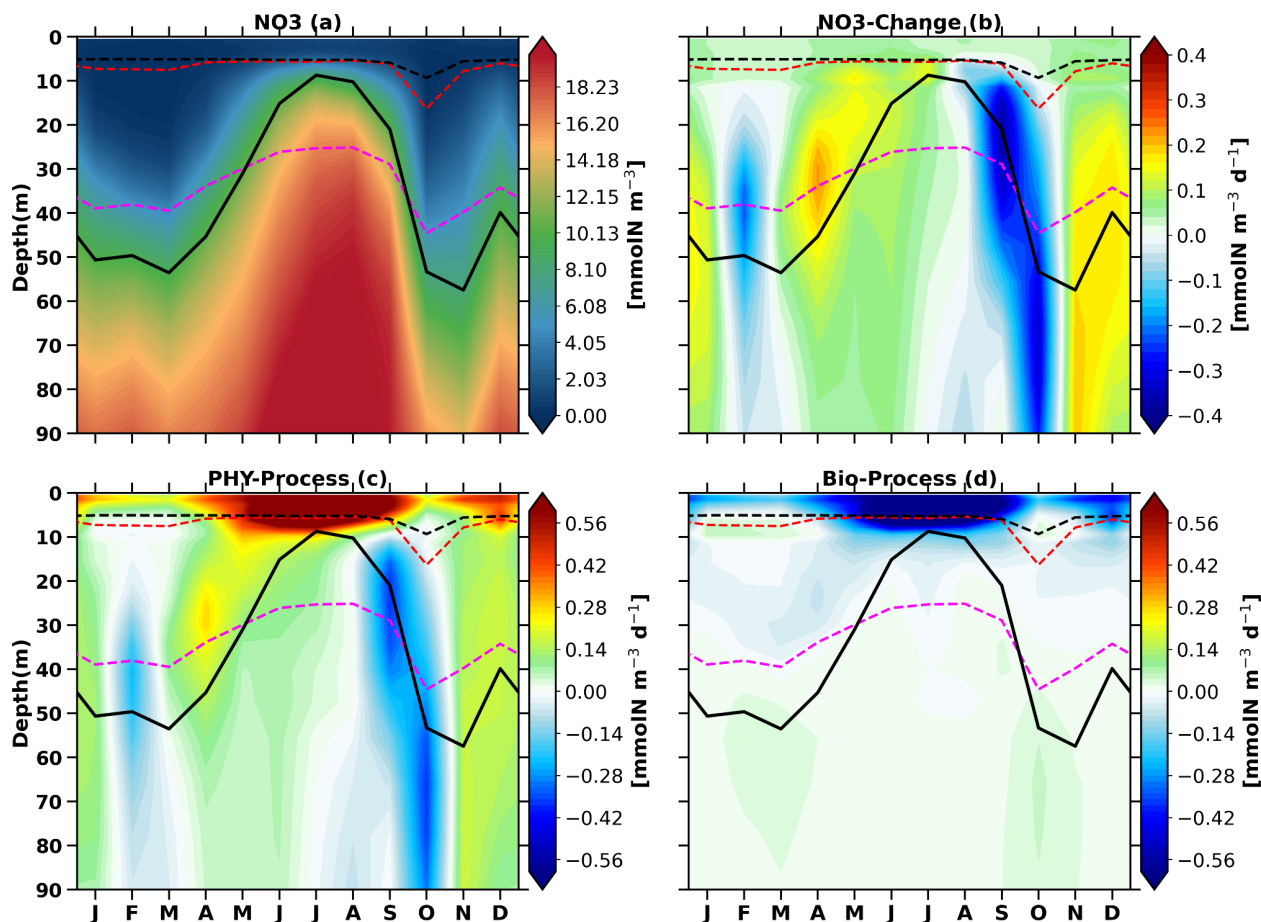


Figure 11. Depth-time Hovmöller diagram of the seasonal cycle of the nitrate budget averaged within the Gabon-Congo coastal box (0–6° S, 1° wide coastal band, as shown in Fig. 1). (a) Nitrate concentration (mmolN m^{-3}), (b) nitrate rate of change, (c) physical process contribution, and (d) biological process contribution ($\text{mmolN m}^{-3} \text{d}^{-1}$). The black solid line represents the thermocline (20 °C isotherm), while dashed magenta, red and black lines indicate the euphotic, isothermal and mixed layer depths, respectively.

($p < 0.05$) with vertical advection, whereas vertical gradient variation has only 0.63 ($p < 0.05$) of correlation with vertical advection. The third component ($w' \cdot \nabla_z(\text{NO}_3)'$, Fig. 15f) has a lower negative correlation -0.062 ($p < 0.05$) with vertical advection. During the upwelling period, the variation in vertical gradient (Fig. 15e) at the base of the mixed layer has a much greater influence on nitrate supply than the variation in vertical velocity (Fig. 15e). Another observation is that in the same main upwelling period there is a lag between maximum vertical current which happens in May and the maximum vertical gradient indicated by the shallowest thermocline in July. This lag results in a highest input of nitrate by vertical advection (Fig. 15a) in the mixed layer in June. It can be seen that the nitrate output by vertical advection during the downwelling period is mostly induced by the vertical nitrate gradient in the mixed layer whereas deeper in the euphotic layer these losses are induced by vertical downward velocities induced by downwelling CTWs propagation.

4 Discussion

In this section, we discuss our results: the model-data comparison, the influence of the mixed layer criteria, the main nitrate budget drivers in the Gabon-Congo upwelling system compared to the other tropical Atlantic upwelling systems. Finally, we will explore the factors governing seasonal productivity in the Gabon-Congo upwelling system, integrating our understanding of physical forcing and nutrient availability to characterize its biological response. Through this comprehensive discussion, we aim to provide a nuanced understanding of the oceanographic processes at play in the coastal Congo region and the capabilities and limitations of our modeling approach.

Throughout this work, we have shown that our model reasonably reproduces the observations in terms of temperature, nitrate, CHLa, SLA and surface currents, although there are a few differences that we will discuss in this section. First of all, we saw that temperature in our model is warmer than observed by around 1 °C in regional distribution (Fig. 2a, b) as

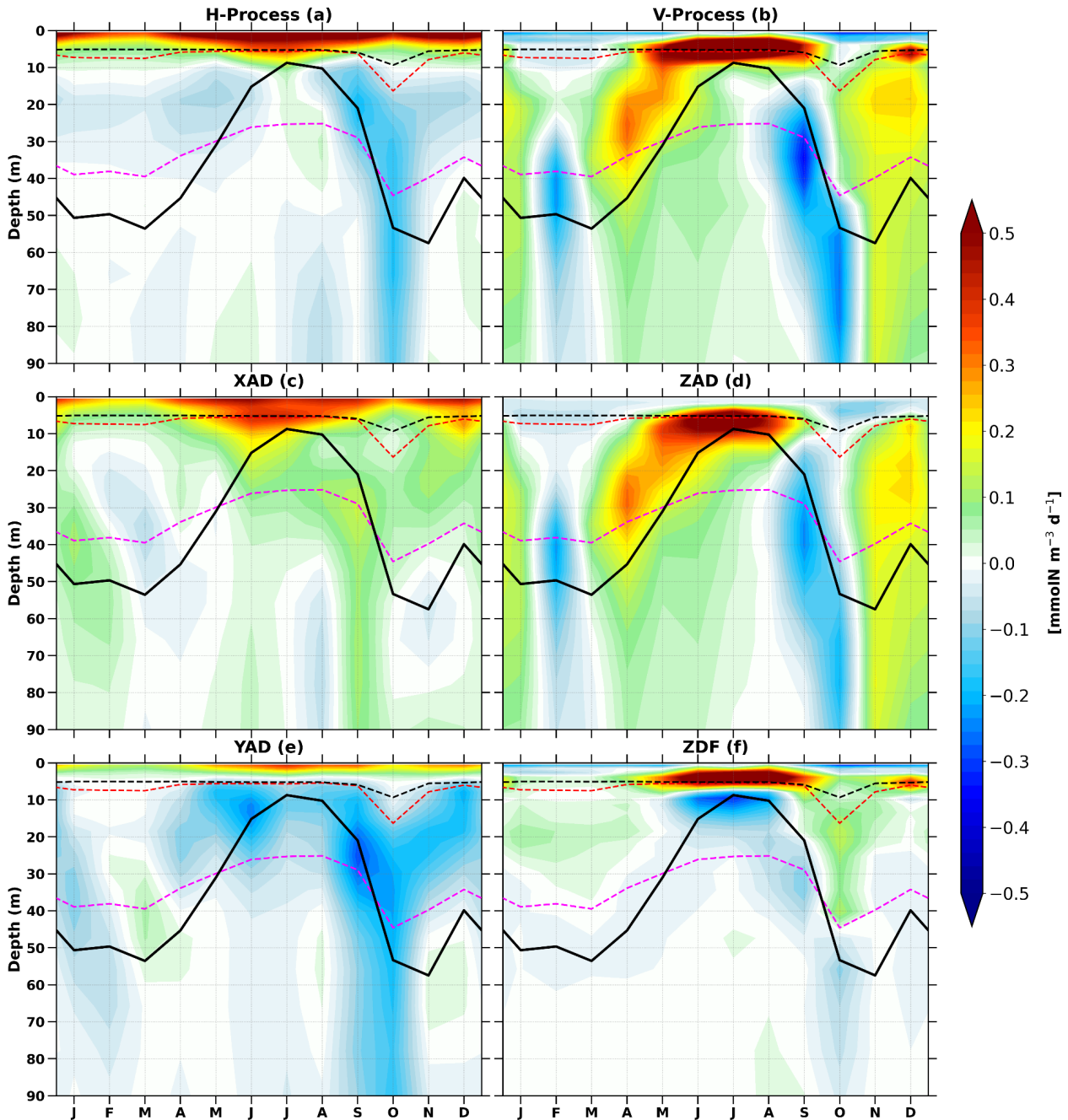


Figure 12. Depth-time Hovmöller diagram of the model seasonal cycle of contributions to the nitrate budget of horizontal and vertical processes ((a) and (b) respectively), zonal, meridional, vertical advections ((c), (e) and (d) respectively), vertical diffusion (f) along the Gabon-Congo coast (0° – 6° S and 1° width to the coast). Units are mmolN m^{-3} for all of the plots. The black solid line represents the thermocline (20°C isotherm), while dashed magenta, red and black lines indicate the euphotic, isothermal and mixed layer depths, respectively.

well as in seasonal cycles (Fig. 4c, d). This is a common bias in ocean and climate models in the Eastern tropical Atlantic (Richter, 2015; Zuidema et al., 2016; Voltaire et al., 2019). Indeed, several studies suggest that this warm bias is multicausal. While it is partly attributed to models' deficiency in simulating low-level clouds, resulting in overestimation of shortwave radiation (Xu et al., 2014), other factors play

a critical role. These include errors in atmospheric forcing, specifically the misrepresentation of the coastal low-level jet and wind stress, which can weaken coastal upwelling (Cabos et al., 2017; Voltaire et al., 2019). Furthermore, complex air-sea feedback mechanisms (Koseki et al., 2018) and difficulties in simulating the vertical thermocline structure in the

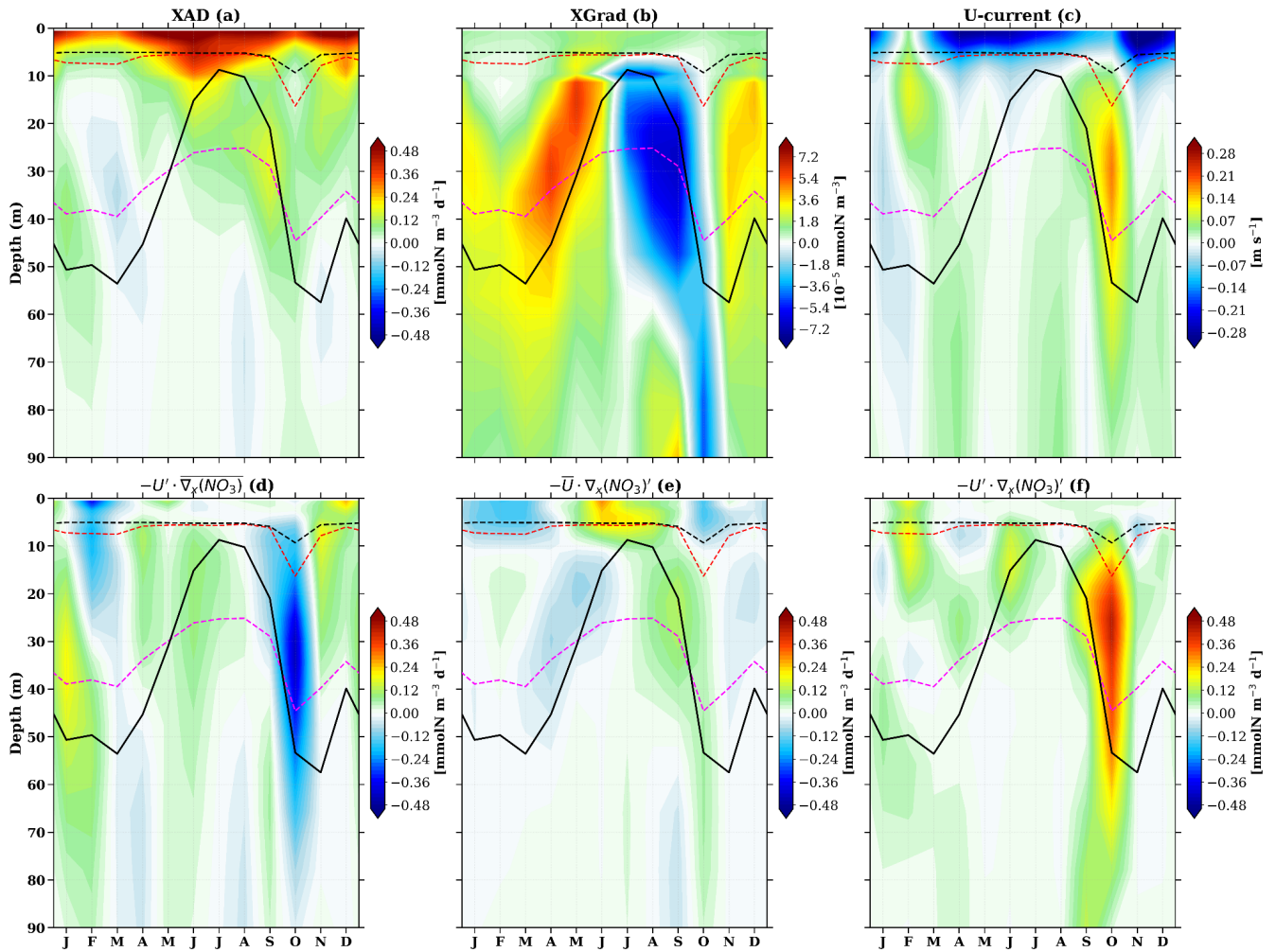


Figure 13. Depth-time Hovmöller diagram of the model seasonal cycle of nitrate advection (a), nitrate gradient (b), zonal current (c), zonal current variation times mean nitrate gradient (d), gradient variation times mean current (e) and gradient variation times zonal current variation (f), all along the zonal axis in the Gabon-Congo coastal box of Fig. 1. Units are milli mol per cubic meter per day for all of the plots except (b) (milli mol per cubic meter) and (c) (meter per second). The black solid line represents the thermocline (20 °C isotherm), while dashed magenta, red and black lines indicate the euphotic, isothermal and mixed layer depths, respectively.

region (Koubanova et al., 2018) are also shared challenges that contribute to this persistent modeling bias.

With regard to nitrate concentrations, the regional distribution shows that north of the mouth of the Congo River and near the coast, the model agrees well with the CARS climatology (Fig. 2c, d). However, offshore and south of the mouth of the Congo River, the model underestimates nitrate concentrations. In the seasonal cycle, we see that the model captures the seasonal variability, but underestimates the amplitude compared to the data. These biases may be explained by the temporal coverage of the CARS climatology, which covers a long period (from 1940 to 2011) of data (Bachèlery, 2016) compared to our model which covers only one year (2011). Another bias may be the lack of data in CARS, in our study area. The differences in the surface CHLa concentration between the model and the satellite observations

may be associated with a lack of data for the ocean colour satellite observations, particularly in August, due to the cloud cover which induces atmospheric contaminations (Hardman-Mountford and McGlade, 2002; Estival et al., 2013) of the satellite signal, resulting in a lack of CHLa signal (Nieto et al., 2017). The biases in the surface currents between the model and the observations are mainly due to the underestimation of the currents in the OSCAR product near the coastal zone (Sikhakolli et al., 2013), especially in our studied area where very few data are available. Despite these results discussed earlier in this paper, we have to keep in mind that there are also some limitations in our simulation. For example, the model has difficulties reproducing the seasonal cycle of CHLa concentration, in particular the first CHLa blooms occurring in February–March, highlighted by the MODIS ocean colour satellite data. This might be due to the CHLa

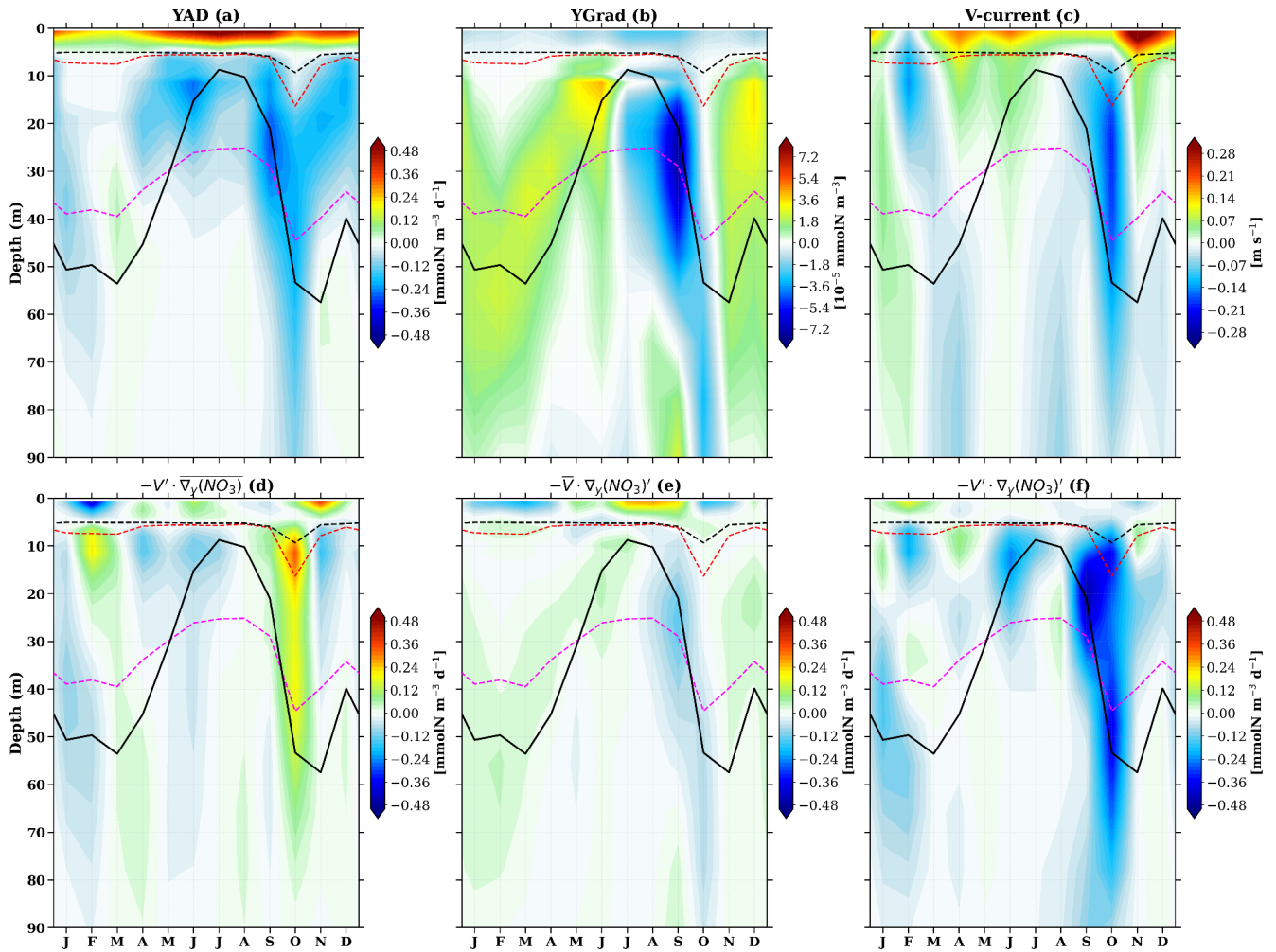


Figure 14. Depth-time Hovmöller diagram of the model seasonal cycle of nitrate advection (a), nitrate gradient (b), meridional current (c), meridional current variation times mean nitrate gradient (d), gradient variation times mean meridional current (e) and gradient variation times current variation (f), all along the meridional axis in the Gabon-Congo coastal box of Fig. 1b. Units are milli mol per cubic meter per day for all of the plots except (b) (milli mol per cubic meter) and (c) (meter per second). The black solid line represents the thermocline (20°C isotherm), while dashed magenta, red and black lines indicate the euphotic, isothermal and mixed layer depths, respectively.

concentration of the Congo river in our model. Indeed, we take into account the nutrients and dissolved organic matter discharges of the river but not the CHLa concentrations (information not available in the HYBAM database). We can also observe a minimal or slightly reduced concentration of CHLa around the mouth of the Congo River in our model (Fig. 2e). This is explained by the very high speed (greater than 2 m s^{-1}) of the Congo River current at its mouth in our model. This has resulted in the transport of CHLa produced by phytoplankton photosynthesis away from the mouth of the Congo River.

Our analysis shows that, in the Gabon-Congo upwelling system, the nitrate budget in the mixed layer is dominated by physical processes during the upwelling period (Fig. 7c), particularly vertical diffusion (Fig. 8f), while zonal advection and vertical mixing play a secondary role. In agreement

to these latter results, Ngakala et al. (2025) using a high resolution simulation ($1/36^{\circ}$) of NEMO in the Gabon-Congo upwelling, have shown through a mixed layer heat budget, that vertical diffusion was the main contributor of cooling during upwelling period in the mixed layer. They found that the vertical advection has a secondary role in cooling of the mixed layer. They state that, if defining instead the mixed layer depth with the Boyer-Montégut criterion, then vertical advection would play a greater role than vertical diffusion. Thus, as mentioned in our study and in agreement with Ngakala et al. (2025), the relative contributions of vertical advection and diffusion depend on the definition of the mixed layer depth.

Our analysis reveals that the seasonal variability of CHLa in our region is driven by the seasonal concentration of nitrate, as in other tropical Atlantic upwelling systems

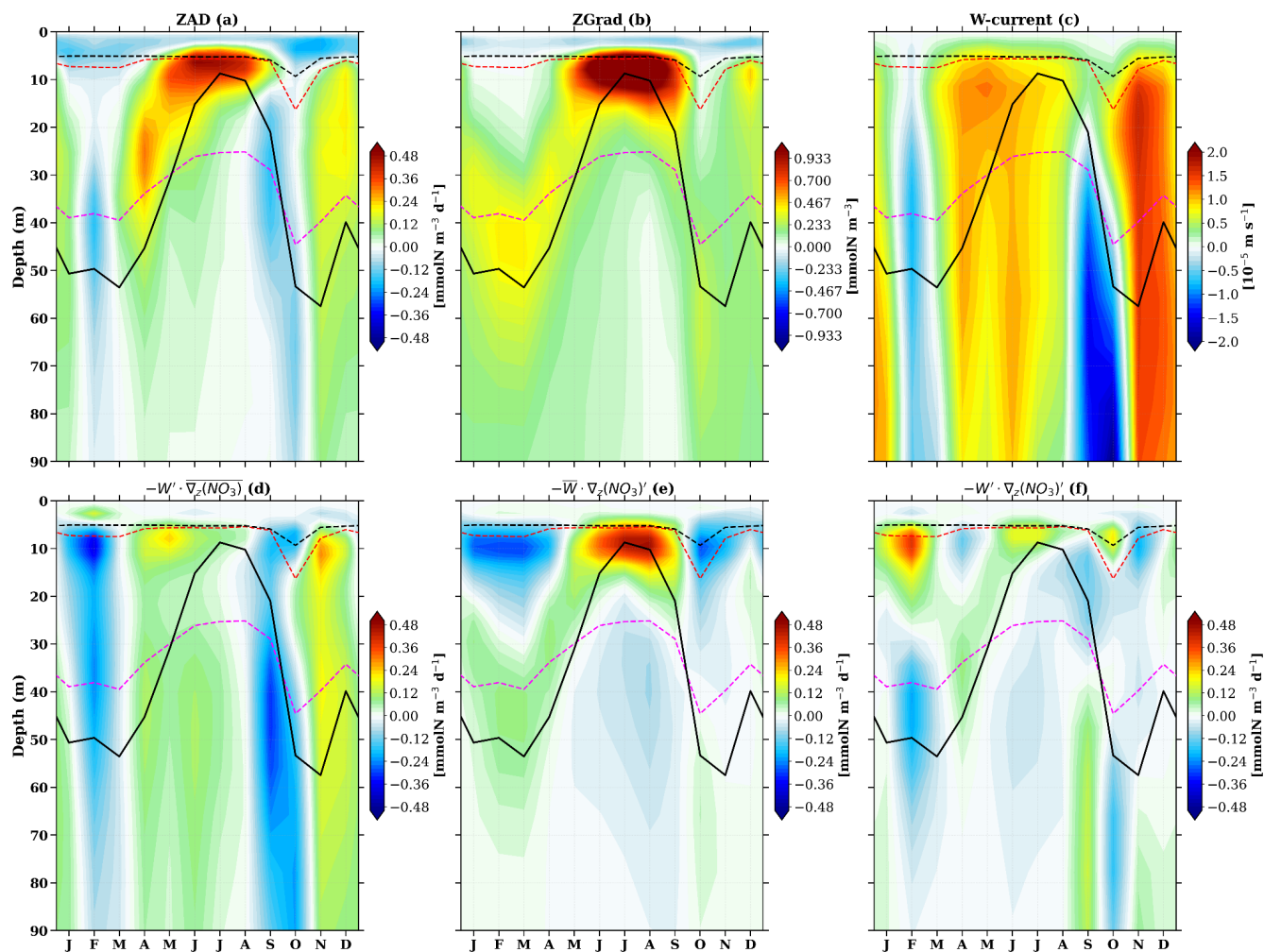


Figure 15. Depth-time Hovmöller diagram of the model seasonal cycle of nitrate advection (a), nitrate gradient (b), vertical current (c), vertical current variation times mean nitrate gradient (d), gradient variation times mean vertical current (e) and gradient variation times current variation (f), all along the vertical axis in the Gabon-Congo coastal box of Fig. 1b. Units are milli mol per cubic meter per day for all of the plots except (b) (milli mol per cubic meter) and (c) (meter per second). The black solid line represents the thermocline (20°C isotherm), while dashed magenta, red and black lines indicate the euphotic, isothermal and mixed layer depths, respectively.

(Radenac et al., 2020). However different processes drive the seasonal cycle of nitrate and CHLa in the different tropical Atlantic upwelling systems. In the Equatorial Atlantic upwelling system, the seasonal cycle of nitrate and CHLa are driven by the wind stress and wind stress curl (Caniaux et al., 2011; Radenac et al., 2020). In the Tropical Angola Upwelling system, the main driver of these seasonal cycle are the CTWs as in our area with a main peak in austral winter (May–July) and a second peak in December–January. However vertical mixing plays also a key role in the Tropical Angola Upwelling system (Awo et al., 2022; Ostrowski et al., 2009; Körner et al., 2023) due to onshore propagating internal tide waves interacting with sloping topography (Brandt et al., 2023). In the upwelling systems of the equatorial Atlantic and tropical Angola, vertical mixing is the main driver of nitrate input to the mixed layer. This is due to local mech-

anisms that occur in these areas (local forcing), such as the intensification of the vertical shear stress between the South Equatorial Current (SEC) and the Equatorial Undercurrent (EUC) at the equator (Jouanno et al., 2011; Radenac et al., 2020) and the dissipation of internal tide that interact with the continental shelf and produce turbulent mixing at the Angolan coast (Körner et al., 2023; Zeng et al., 2021; Brandt et al., 2023). In the Gabon-Congo system, we can suggest that the strong stratification induced by the discharge of the Congo River, which is the second largest river in the world, contributes to thinning the mixed layer, limiting the effect of mixing very close to the surface (Dossa et al., 2019).

In the euphotic layer and below, the nitrate budget is almostly dictated by physical processes, which are mainly modulated by currents that transport water of different properties. We noted that vertical and zonal advections were the

drivers of nitrate input in the upwelling period, while vertical mixing and meridional advection were the drivers of nitrate losses in the lower part of the euphotic layer (just below the mixed layer depth) in this period. However, during the downwelling period, vertical mixing mostly brings nitrate to the lower part of the euphotic layer, while vertical and meridional advection always remove nitrate. Meridional advection is therefore the main factor in nitrate loss in the euphotic layer all year long. This is consistent with the warming effect of meridional advection shown by Körner et al. (2023) in the Angolan upwelling. Radenac et al. (2020) showed that in the equatorial euphotic layer, zonal advection by the EUC current was the main driver of nitrate losses, which may explain our previous results since the southward Angola current dominating the ocean circulation in the Congo-Angola zone is fed by the EUC current. Indeed, the EUC, whose source waters come from the oligotrophic layers of the subtropical South Atlantic, has relatively low nitrate concentrations compared to neighbouring waters (Schott et al., 1998; Johns et al., 2014; Tuchen et al., 2022). These low nitrate waters are brought to the Congo-Angola system by the Angola Current (AC) (Fig. 16), reducing nitrate concentration in the euphotic layer. At the same time, the AC brings CHLa into the euphotic layer by meridional advection, as the EUC has relatively high CHLa concentrations (Radenac et al., 2020). This low nitrate/high CHLa signature of the AC can be seen in the first hundred metres and in particular at the base of the euphotic layer along the Gabon-Congo coast (Fig. A1c), where the AC flows (Kopte, 2017). Further analyses show that the coastal CHLa maximum occurs from May to September with a peak in August, which is consistent with the seasonal cycle of the CHLa concentration in the EUC (Radenac et al., 2020; Brandt et al., 2023). The simultaneous variation in current and gradient appears to be the main factor contributing to variations in the meridional advection and nitrate removal, mainly between July and October. Over the same period, we observe a sign change of the meridional nitrate gradient (Fig. 14b), which is generally positive (indicating that under the mixed layer, waters to the south of the coastal box (0°N – 6°S , 1° width from the coast; see Fig. 1b) are less nitrate-rich than waters to the north) under the mixed layer from January to June.

This observation suggests that for the period from September to October, waters in the southern part of the box are now richer in nitrate than waters in the northern part of the box under the mixed layer. Beyond horizontal transport, this frontogenesis is also driven by the meridional gradient of vertical motion ($\partial w/\partial y$). A stronger upward vertical velocity in the southern section (near 6°S) compared to the north leads to a higher vertical nitrate supply in the south, establishing the negative meridional nitrate gradient observed in Fig. 14b. This highlights the important role of vertical processes in the regional enrichment, as also emphasized by Nubi et al. (2016) for the equatorial band. This also reflects the passage of low-nitrate waters from the EUC via the An-

gola Current to the Gabon-Congo coast. However, we find that zonal advection brings nitrate in the euphotic layer and its decomposition has shown that its variation is mostly influenced by zonal nitrate gradient variation, with a secondary contribution of zonal current variation. This zonal current variation is seen to remove nitrate in the euphotic layer during February–March and July–October. We can also see that in these periods the zonal current flows toward the coast, which suggests that it brings low nitrate water from offshore toward the coast. This seasonally eastward current is consistent with the seasonal cycle of SEUC (Siegfried et al., 2019; Assene et al., 2020). Besides this, we can also see that there is a sign change of the zonal nitrate gradient (Fig. 13b) which occurs simultaneously with the sign change of the meridional nitrate gradient (Fig. 14b) suggesting that this inversion in zonal nitrate gradient is due to Angola Current water at the coast. In fact, this later result highlights that the Angolan Current waters flowing along the coast are less rich in nitrate than the water brought from offshore toward the coast by the SEUC. As nitrate concentration in the coast is lower, SEUC waters act to increase nitrate concentration in our coastal box, through zonal advection in the euphotic layer from April to December. The CHLa budget analysis (Appendix A, Fig. A1) shows that the SEUC brings through zonal advection low CHLa water at the coast thereby reducing the nitrate input during the downwelling period. In the nitrate budget we saw that the main driver of nitrate input was vertical advection associated with CTWs. Körner et al. (2024) have shown, using satellite and mooring data, that CTWs detected in the SLA are of the low vertical mode, while the movement of the isopycnals is rather consistent with the vertical velocity structure of higher modes. This explains why isopycnals reach their seasonal minimum/maximum depth (in phase with the nitracline) after the minimum in SLA (Körner et al., 2024). The spatial distribution of mean annual nitrate and CHLa concentrations (Fig. 16a, b) provides clear evidence of the influence of the Angola Current (AC) on the coastal biogeochemistry of the Gabon-Congo system. Physically, the AC is a southward-flowing coastal current that advects warm, equatorial-origin waters along the shelf. Biogeochemically, our model results (Fig. 16a) show that while the broader coastal box is enriched in nutrients due to upwelling and riverine inputs, there is a distinct relative decrease in nitrate concentrations strictly along the shoreline, particularly south of 5°S . In this narrow coastal band, NO_3 values are lower than those found in the core of the upwelling plume located slightly further offshore. Conversely, the chlorophyll *a* map (Fig. 16b) reveals a robust coastal belt with maximum concentrations exceeding 4.5 mg m^{-3} right at the coast. This low-nitrate/high-CHLa inverse relationship at the immediate coastline is consistent with the known characteristics of the Angola Current. Indeed, the AC transports mature waters originating from the Equatorial Undercurrent (EUC).

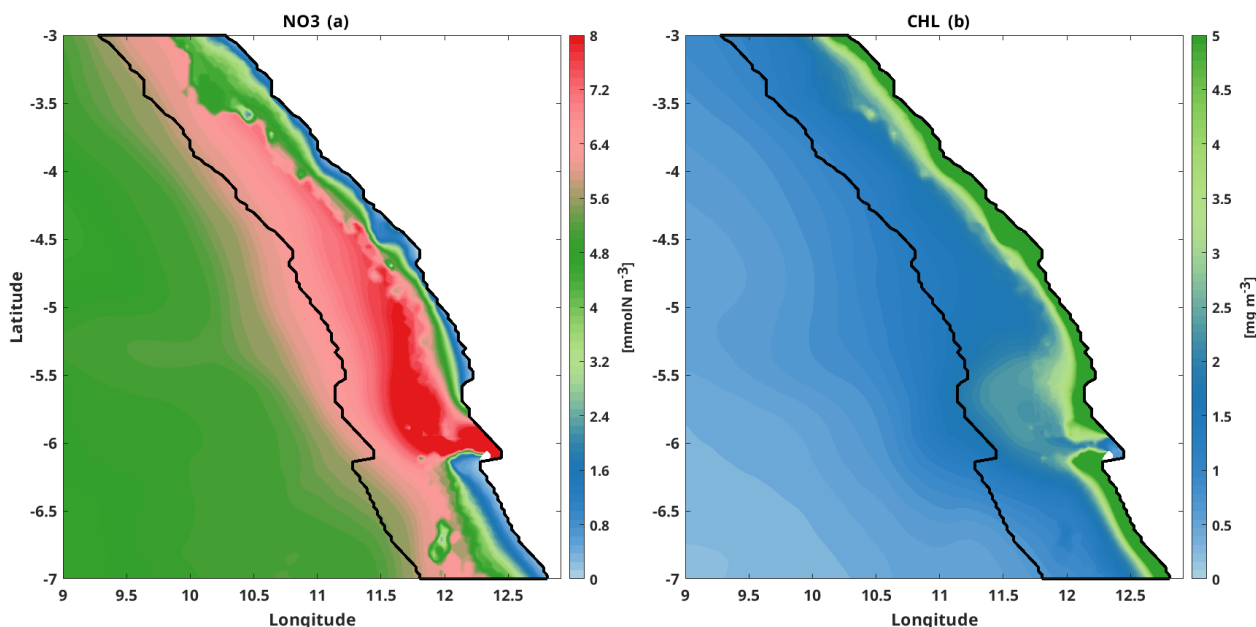


Figure 16. Regional distribution of mean annual nitrate and CHLa concentration ((a), (b) respectively) averaged on the 0–100 m layer along the Gabon-Congo upwelling area, black line represents different boundaries of our Coastal box with a width of 1° of longitude relative to the coast.

We assessed the variability of biological productivity using the PISCES component of our coupled model (Fig. 18). The results show a clear semi-annual cycle of Net Primary Production (NPP), New Production (NP), and Regenerated Production (RP), which is consistent with the seasonal cycle of nitrate and CHLa concentrations observed in the region (Körner et al., 2024). The highest values of NPP (Fig. 17a) are found near the Congo River mouth (between 5.5 and 6° S), where average values exceed $0.20 \text{ mol N m}^{-2} \text{ d}^{-1}$. During the main upwelling period (June–August), the NPP reaches its maximum, with local peaks near 6° S exceeding $0.25 \text{ mol N m}^{-2} \text{ d}^{-1}$. This intensity is comparable to, though slightly lower than, the average primary production reported for the Benguela and Humboldt systems, which reach 0.37 and $0.33 \text{ mol N m}^{-2} \text{ d}^{-1}$ respectively (converted from Tilstone et al., 2009; Monteiro et al., 2011).

The secondary upwelling period in December also shows high productivity, with NPP values reaching approximately $0.22 \text{ mol N m}^{-2} \text{ d}^{-1}$ near the river mouth. In contrast, during the downwelling periods (notably in March and October), the system becomes less productive, with NPP dropping below $0.075 \text{ mol N m}^{-2} \text{ d}^{-1}$ in most of the coastal box. The analysis of production components reveals that during the main upwelling season, the New Production (NP) (Fig. 17b) peaks at around $0.15 \text{ mol N m}^{-2} \text{ d}^{-1}$, representing about 50%–60% of the NPP. In December, the NP contribution is lower, around $0.10 \text{ mol N m}^{-2} \text{ d}^{-1}$. The Regenerated Production (RP) (Fig. 17c) remains a significant and stable driver of productivity throughout the year, particularly near the Congo mouth where it often exceeds $0.125 \text{ mol N m}^{-2} \text{ d}^{-1}$, high-

lighting the importance of nutrient recycling in this river-influenced system.

High values of Net Primary Production (NPP) are also observed around 4.47° S, near the mouth of the Kouilou River, following the characteristic semi-annual cycle of the region. A detailed comparison of the production components (Fig. 17b, c) reveals that Regenerated Production (RP), fueled by the recycling of nutrients within the euphotic layer, is generally higher than New Production (NP). These two parameters remain consistent with the seasonal cycle of nitrate concentrations described previously.

The seasonal cycle of NPP in the Gabon-Congo system differs from those of the Benguela upwellings (including the Namibian area), which are primarily wind-forced systems (Gutknecht et al., 2013). A key distinction lies in the efficiency of nitrate utilization: in our study area, the contribution of New Production to the total NPP is notably high. For instance, while the f -ratio (NP / NPP) in the Benguela system typically ranges between 0.2 and 0.4 (Monteiro et al., 2011), it reaches approximately 0.6 in the Gabon-Congo coastal box, indicating that more than half of the primary production is sustained by the upward supply of new nitrates.

Finally, we demonstrate that the conclusions regarding the nitrate budget are highly sensitive to the definition of the Mixed Layer Depth (MLD). In this study, we adopted a 3 m reference depth for the MLD calculation, following the criterion proposed by Aroucha et al. (2025). This shallower definition is more appropriate for the Gabon-Congo system, as it accurately captures the intense surface stratification induced by the river's freshwater plume. With this

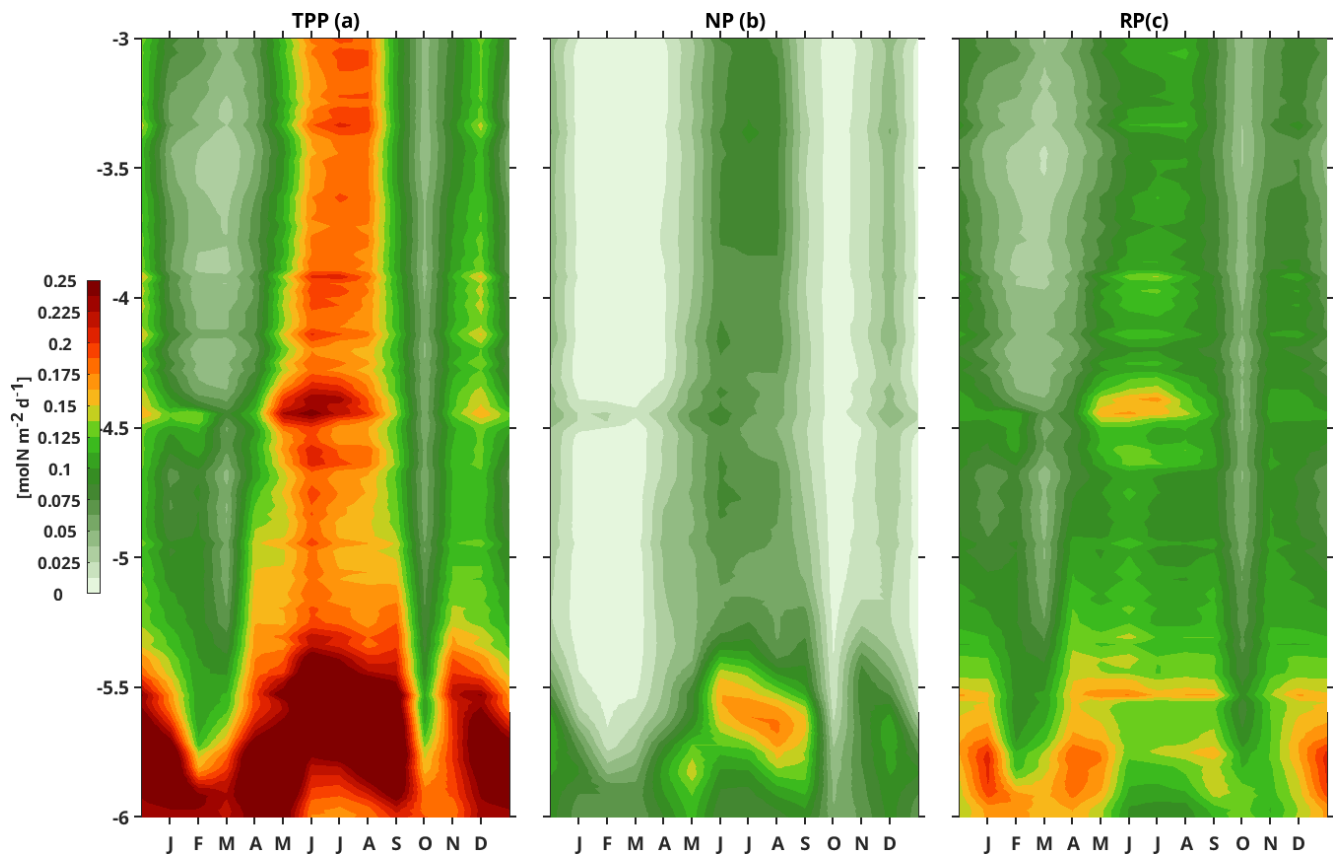


Figure 17. Latitude-Time Hovmöller diagram of biological productivity: Net Primary Production (a), New Production (b) and regenerated Production (c) in the coastal box ($6\text{--}3^\circ\text{S}$, 1° wide along the coastline). The units are milli mol per cubic meter per day.

refined MLD criterion, our results show a significant shift in the balance of vertical processes: vertical diffusion (mixing) now emerges as the dominant mechanism supplying nitrate to the mixed layer, outweighing the contribution of vertical advection. This finding aligns with recent observations in the Angolan upwelling (Brandt et al., 2023; Körner et al., 2023, 2024) and the Gabon-Congo plume region (Scannell and McPhaden, 2018; Ngakala et al., 2025), which highlight turbulent mixing – often fueled by internal tides and shear – as a major driver of vertical nutrient and heat fluxes. This shift emphasizes the critical role of the “Barrier Layer” and the strong surface halocline in trapping nutrients and modulating their upward transfer through small-scale mixing processes rather than mean vertical motion.

5 Conclusions

Throughout this work we have described and analysed the seasonal cycles in nitrate and CHL_a concentrations, as well as the physical and biological processes that modulate nitrate supply and biological productivity in the mixed layer and in the euphotic layer in the Gabon-Congo upwelling system. We began by validating a regional high-resolution

($1/36^\circ$) simulation of the coupled physical-biogeochemical model NEMO-PISCES in this area for the studied year 2011. Surface and subsurface validation of the simulation using observations (satellite, in situ, climatology) shows that the model reasonably reproduces the main physical and biogeochemical characteristics of the study area. Subsequently, the seasonal cycle of nitrate shows that there are two periods of upwelling and two periods of downwelling (Figs. 4e, f and 11a). These upwelling and downwelling are associated with remote forcing: Kelvin waves that propagate along the equator and the coastal waveguide force the vertical migrations of the thermocline, which is also a proxy for the nitracline. The seasonal cycle of CHL_a is explained by that of nitrate. The assessment of the nitrate balance in the mixed layer shows that the main nitrate is mainly supplied in the mixed layer by vertical diffusion (Fig. 10f), vertical advection (Fig. 10d) and zonal advection (Fig. 10c), which is mainly modulated by nitrate inputs from the Congo River at 6°S . The vertical advection induced by CTWs and vertical diffusion play also a role in the nitrate supply, while nitrate losses are linked to meridional advection and the biological activity (photosynthesis). In the lower part of the euphotic layer, on the other hand, nitrate is supplied by zonal advection and vertical ad-

vection. Vertical diffusion contributes to nitrate losses, except in downwelling periods where it represents one of the main drivers of nitrate supply. We have also seen that meridional advection via the Angola Current, which transports the low-nitrate warm waters of the Equatorial undercurrent, is the main driver of nitrate loss below the mixed layer throughout the year. We find that vertical advection is controlled by the vertical nitrate gradient and nitrate input (Fig. 15), rather than vertical velocity, when it brings nitrate into the mixed layer during the main upwelling period. However, in the secondary upwelling in December, vertical advection also brings nitrate, but is then mostly controlled by vertical velocity.

In future works, the interannual variability will be studied, specifically in association with the interannual variability of the Congo River discharges (Scannell and McPhaden (2018), Körner et al., 2023, 2024; Brandt et al., 2023) and of the CTWs forced by the Equatorial Kelvin waves (e.g. Bachèlery et al., 2015; Bachèlery, 2016). Understanding the seasonal and interannual variability of productivity is of primary interest to ensure the sustainability of ecosystems and fisheries in the Gabon-Congo upwelling system.

Appendix A: Euphotic Layer CHLa Budget Analysis

In the lower part of the euphotic zone, the CHLa budget (Fig. A1) is primarily governed by the interaction between coastal and offshore water masses. During the downwelling period, the zonal advection term (XAD_CHL) shows a net loss of CHLa near the base of the euphotic layer. This is explained by the passage of the South Equatorial Undercurrent (SEUC). As described by Nubi et al. (2016), undercurrent waters (EUC/SEUC) are relatively nitrate-poor and carry less CHLa than the highly productive coastal waters. The eastward transport of these offshore waters towards the Gabon-Congo coast leads to a dilution of the local CHLa concentration, a process captured by the negative values in the zonal advection budget.

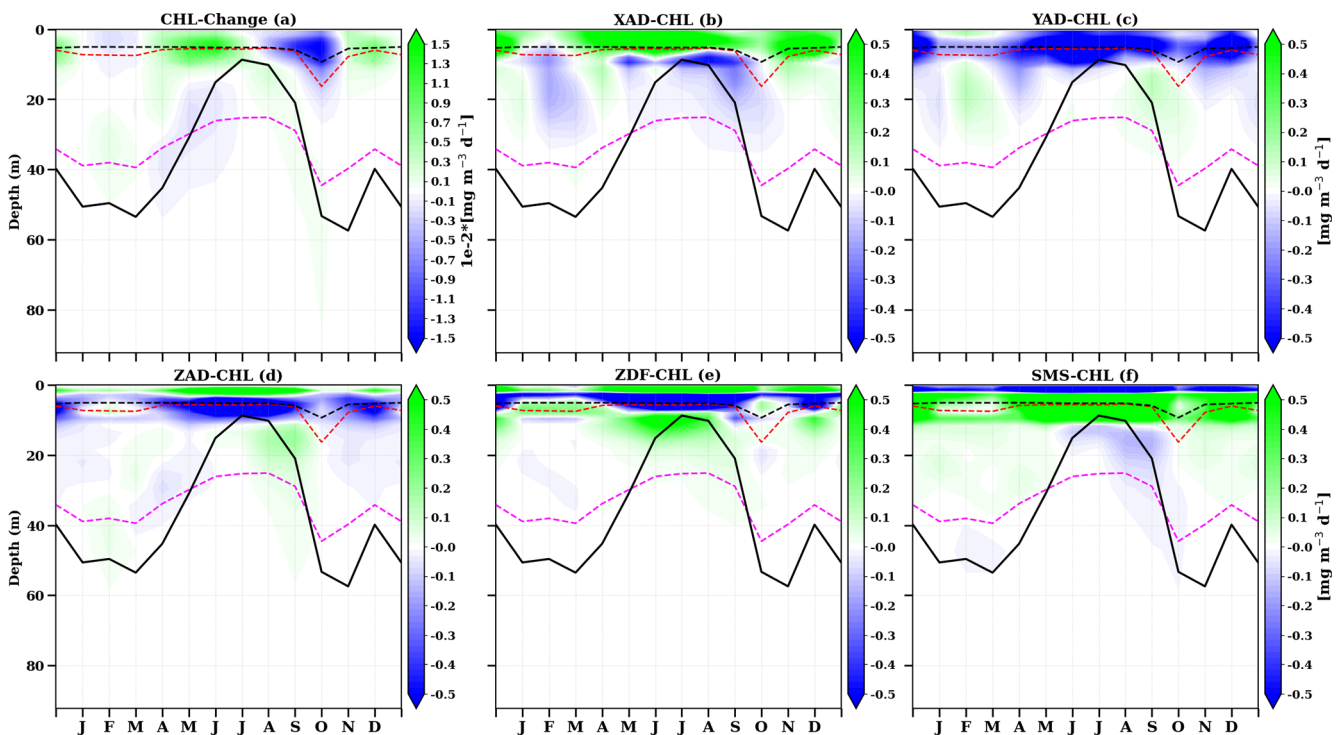


Figure A1. Depth-time Hovmöller diagram of the seasonal chlorophyll *a* budget along the Gabon-Congo coast (6°S – 0°N , 1° coastal strip) for: (a) total rate of change (CHL-change), (b) zonal advection (XAD-CHL), (c) meridional advection (YAD-CHL), (d) vertical advection (ZAD-CHL), (e) vertical diffusion (ZDF-CHL), and (f) biological source-minus-sink term (SMS-CHL). Units for all panels are $\text{mg m}^{-3} \text{d}^{-1}$. The black solid line represents the thermocline (20°C isotherm), while dashed magenta, red and black lines indicate the euphotic, isothermal and mixed layer depths, respectively.

Appendix B: Euphotic Layer Nitrate Advections Components Analysis

To further investigate this relationship, the individual contributions of seasonal current and gradient variations are shown in Appendix B (Fig. B1). This decomposition confirms that the mean flow acting on seasonal gradient anomalies is the dominant driver of advection variability.

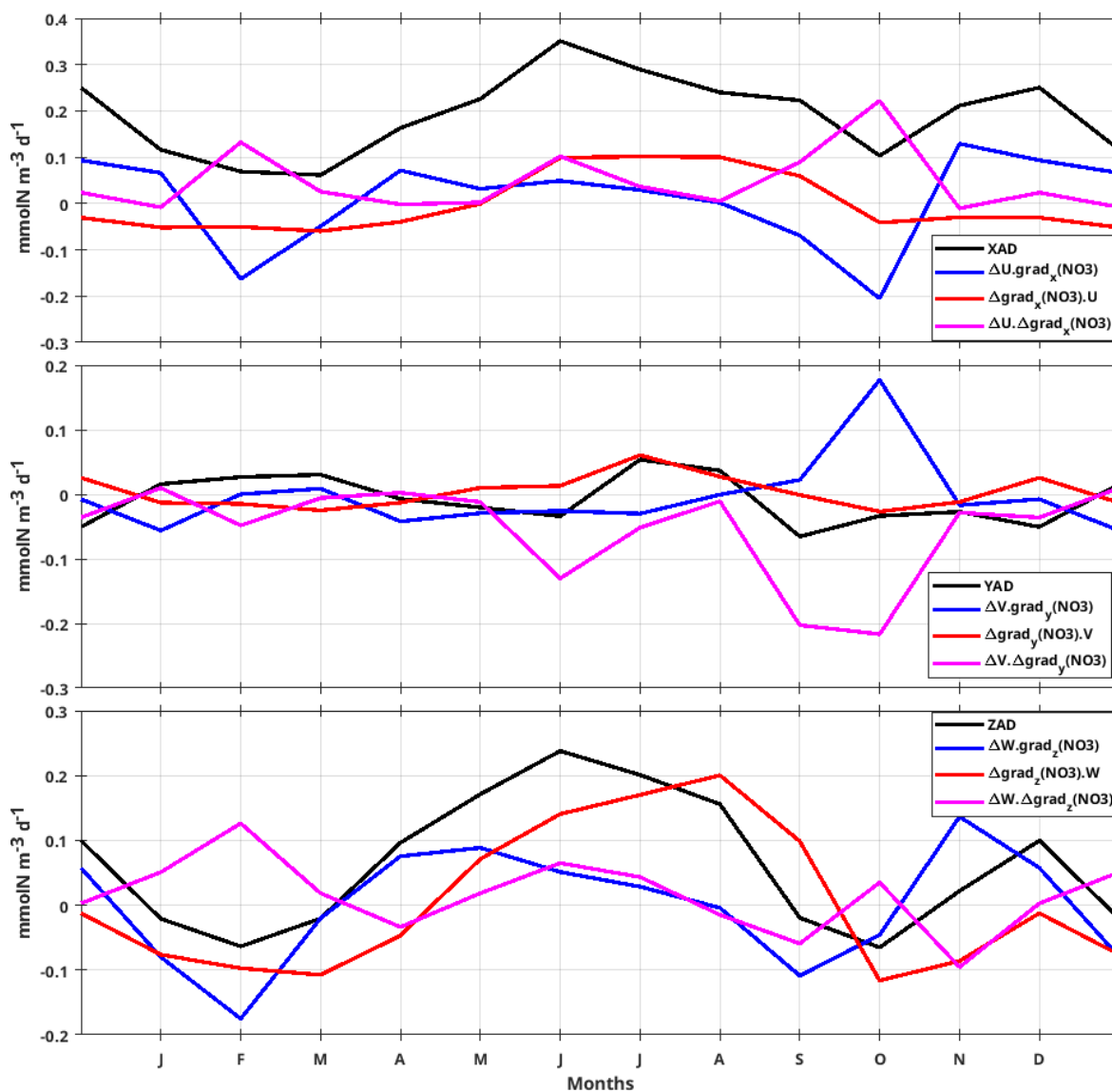


Figure B1. Seasonal variation of advection components averaged in the euphotic layer, black line represent zonal, meridional and vertical advection in (a), (b) and (c) respectively. The red line in both three figures represents gradient variation, blue line is current variation and magenta line represents the simultaneous variation of gradient and current.

Appendix C: Acronyms

CTW:	Coastally trapped waves
CoUS:	Gabon-Congo Upwelling System
EKW:	Equatorial Kelvin Waves
GG:	Gulf of Guinea
MLD:	Mixed Layer Depth
SST:	Sea Surface Temperature
SSH:	Sea Surface Height
SLA:	Sea Level Anomaly
CHLa:	Chlorophyll <i>a</i>
EBUS:	Eastern Boundary Upwelling System
TAUS:	Tropical Angolan Upwelling System

Code and data availability. Publicly available datasets were used for this study. Chlorophyll data (1998–2020) are from the Copernicus-GlobColour dataset (<https://doi.org/10.48670/moi-00281>, Copernicus Marine Service, 2023a). The sea level anomaly data (1998–2020) were accessed via the Copernicus Server (<https://doi.org/10.48670/moi-00148>, Copernicus Marine Service, 2023b). The MUR SST product created by the JPL MUR MEaSURES program as part of the GHRSSST (Group for High-Resolution Sea Surface Temperature) project is obtained from <https://doi.org/10.5067/GHGMR-4FJ04> (JPL MUR MEaSURES Project, 2015; Chin et al., 2017) and ASCAT wind data <https://podaac.jpl.nasa.gov/dataset/ASCATB-L2-25km> (last access: 11 April 2026). The nutrient fields were assessed using the CSIRO Atlas of Regional Seas climatology (Dunn and Ridgway, 2002), <https://portal.aodn.org.au/search?uuid=d9302a48-57b1-41c2-a0dc-78bd00dd5e4b> (last access: 11 April 2026). Near surface currents from the Ocean Surface Current Analysis Real-time (OSCAR, Johnson et al., 2007), <https://doi.org/10.5067/OSCAR-25I20> (ESR and Dohan, 2022) ESR. Model outputs are available from the authors, especially GA, ID, GM, and JJ.

The processed data and scripts used in this study are available in the Zenodo repository at <https://doi.org/10.5281/zenodo.19384386> (Mbang Essome et al., 2026).

Author contributions. LJME outlined and wrote the paper. LJME and RDG produced the figures. GM has run the NEMO-PISCES model. GA, ID, CYD the co-authors contributed to define methodology and reviewed the paper.

Competing interests. The contact author has declared that none of the authors has any competing interests.

Disclaimer. Publisher's note: Copernicus Publications remains neutral with regard to jurisdictional claims made in the text, published maps, institutional affiliations, or any other geographical representation in this paper. The authors bear the ultimate responsibility for providing appropriate place names. Views expressed in the text are those of the authors and do not necessarily reflect the views of the publisher.

Acknowledgements. Research is sponsored by the CNES SWOT-ETAO project (Surface Water and Ocean Topography, Study of Ocean Topography and Altimetry by the National Centre for Space Studies France). GENCI GEN7298 project (National High-Performance Computing Equipment) for computing hours for simulations.

Thanks go to https://podaac.jpl.nasa.gov/dataset/OSCAR_L4_OC_INTERIM_V2.0 (last access: 11 April 2026) to provide OSCAR current data.

Also thanks to <https://podaac.jpl.nasa.gov/dataset/MUR-JPL-L4-GLOB-v4.1> (last access: 11 April 2026) for providing MUR SST data.

Financial support. This project is funded by the IRD-ARTS program (Allocation de Recherche pour une Thèse au Sud, no. dossier: 153240T) for the PhD scholarship of Landry Junior Mbang Essome.

Review statement. This paper was edited by Damian Leonardo Arévalo-Martínez and reviewed by two anonymous referees.

References

- Aroucha, L. C., Lübbecke, J. F., Brandt, P., Schwarzkopf, F. U., and Biastoch, A.: River discharge impacts coastal south-eastern tropical Atlantic sea surface temperature and circulation: a model-based analysis, *Ocean Sci.*, 21, 661–678, <https://doi.org/10.5194/os-21-661-2025>, 2025.
- Assene, F., Morel, Y., Delpech, A., Aguedjou, M., Jouanno, J., Cravatte, S., Marin, F., Ménesguen, C., Chaigneau, A., Dadou, I., Alory, G., Holmes, R., Bourlès, B., and Koch-larrouy, A.: From Mixing to the Large Scale Circulation: How the Inverse Cascade Is Involved in the Formation of the Subsurface Currents in the Gulf of Guinea, *Fluids*, 5, 147, <https://doi.org/10.3390/fluids5030147>, 2020.
- Aumont, O. and Bopp, L.: Globalizing results from ocean insitu iron fertilization experiments, *Global Biogeochem. Cy.*, 20, GB2017, <https://doi.org/10.1029/2005GB002591>, 2006.
- Aumont, O., Belviso, S., and Monfray, P.: Dimethylsulfide (DMS) cycle with a 3-D ocean-biogeochemical model, *Oceanogr. Lit. Rev.*, 11, 1637, <https://doi.org/10.1029/1999JC000111>, 1998.
- Aumont, O., Ethé, C., Tagliabue, A., Bopp, L., and Gehlen, M.: PISCES-v2: an ocean biogeochemical model for carbon and ecosystem studies, *Geosci. Model Dev.*, 8, 2465–2513, <https://doi.org/10.5194/gmd-8-2465-2015>, 2015.
- Awo, F. M., Alory, G., Da-Allada, C. Y., Delcroix, T., Jouanno, J., Kestenare, E., and Baloïtcha, E.: On the seasonal and interannual variability of the sea surface salinity in the Gulf of Guinea, *Clim. Dynam.*, 60, 2121–2140, <https://doi.org/10.1007/s00382-022-06443-4>, 2023.
- Awo, F. M., Rouault, M., Ostrowski, M., Tomety, F. S., Da-Allada, C. Y., and Jouanno, J.: Seasonal cycle of sea surface salinity in the Angola Upwelling System, *J. Geophys. Res.-Oceans*, 127, e2022JC018518, <https://doi.org/10.1029/2022JC018518>, 2022.
- Bachèlery, M. L.: Variabilité côtière physique et biogéochimique en Atlantique Sud-Est: rôle du forçage atmosphérique local versus téléconnexion océanique, PhD thesis, University of Paul

- Sabatier, Toulouse, France, 215 pp., <https://theses.hal.science/tel-05004928> (last access: 11 April 2026), 2016.
- Bachèlery, M.-L., Illig, S., and Dadou, I.: Interannual variability in the South-East Atlantic Ocean, focusing on the Benguela Upwelling System: Remote versus local forcing, *J. Geophys. Res.-Oceans*, 121, 284–310, <https://doi.org/10.1002/2015JC011168>, 2015.
- Bourlès, B., Molinari, R. L., Johns, W. E., Gouriou, Y., and Carder, K. L.: The South Equatorial Undercurrent in the Atlantic Ocean, *Geophys. Res. Lett.*, 31, L14301, <https://doi.org/10.1029/2004GL020020>, 2004.
- Brandt, P., Alory, G., Awo, F. M., Dengler, M., Djakouré, S., Imbol Koungue, R. A., Jouanno, J., Körner, M., Roch, M., and Rouault, M.: Physical processes and biological productivity in the upwelling regions of the tropical Atlantic, *Ocean Sci.*, 19, 581–601, <https://doi.org/10.5194/os-19-581-2023>, 2023.
- Cabos, W., Sein, D. V., Pinto, J. G., Koseki, S., Álvarez-García, F. J., and Durán-Quesada, A. M.: The coastal upwelling system of the southeast Atlantic as simulated by a high-resolution coupled model, *Clim. Dynam.*, 49, 1809–1828, <https://doi.org/10.1007/s00382-016-3319-9>, 2017.
- Caniaux, G., Giordani, H., Redelsperger, J. L., Guichard, F., Key, E., and Wade, M.: Coupling between the Atlantic cold tongue and the West African monsoon in boreal spring and summer, *J. Geophys. Res.-Oceans*, 116, C04003, <https://doi.org/10.1029/2010jc006570>, 2011.
- Carr, M.-E.: Estimation of potential productivity in Eastern Boundary Currents using remote sensing, *Deep-Sea Res. Pt. II*, 49, 59–80, [https://doi.org/10.1016/S0967-0645\(01\)00094-7](https://doi.org/10.1016/S0967-0645(01)00094-7), 2002.
- Chavez, F. P. and Messié, M.: A comparison of eastern boundary upwelling ecosystems, *Prog. Oceanogr.*, 83, 80–96, <https://doi.org/10.1016/j.pocean.2009.07.032>, 2009.
- Chin, T. M., Vazquez-Cuervo, J., and Armstrong, E.: A multi-scale high-resolution analysis of global sea surface temperature, *Remote Sens. Environ.*, 200, 154–169, <https://doi.org/10.1016/j.rse.2017.07.029>, 2017.
- Copernicus Marine Service: Global Ocean Colour (Copernicus-GlobColour), Multi-year data, Marine Data Store (MDS) [data set], <https://doi.org/10.48670/moi-00281>, 2023a.
- Copernicus Marine Service: Global Ocean Gridded L4 Sea Level Anomalies (DUACS) and Derived Variables, Multi-year data, Marine Data Store (MDS) [data set], <https://doi.org/10.48670/moi-00148>, 2023b.
- Dossa, A., Da-Allada, C., Herbert, G., and Bourlès, B.: Seasonal cycle of the salinity barrier layer revealed in the north-eastern Gulf of Guinea, *Afr. J. Mar. Sci.*, 41, 163–175, <https://doi.org/10.2989/1814232X.2019.1616612>, 2019.
- Ducet, N., Le Traon, P.-Y., and Reverdun, G.: Global high-resolution mapping of ocean circulation from TOPEX/Poseidon and ERS-1 and -2, *J. Geophys. Res. Oceans*, 105, 19477–19498, <https://doi.org/10.1029/2000jc900063>, 2000.
- Dunn, J. R. and Ridgway, K. R.: Mapping ocean properties in regions of complex topography, *Deep-Sea Res. Pt. I*, 49, 591–604, [https://doi.org/10.1016/S0967-0637\(01\)00069-3](https://doi.org/10.1016/S0967-0637(01)00069-3), 2002.
- ESR and Dohan, K.: Ocean Surface Current Analyses Real-time (OSCAR) Surface Currents – Interim 0.25 Degree (Version 2.0), Ver. 2.0. PO.DAAC [data set], CA, USA, <https://doi.org/10.5067/OSCAR-25120>, 2022.
- Estival, R., Quiniou, V., and Messenger, C.: Real-time network of weather and ocean stations: public-private partnership on in-situ measurements in the Gulf of Guinea, *Sea Technol.*, 54, 34–38, 2013.
- FAO: Fishery and Aquaculture Country Profiles, Angola, Country Profile Fact Sheets, Fisheries and Aquaculture Division, <https://www.fao.org/fishery/en/facp/ago?lang=en> (last access: 11 April 2023), 2022.
- Fréon, P., Barange, M., and Arístegui, J.: Eastern boundary upwelling ecosystems: integrative and comparative approaches, *Prog. Oceanogr.*, 83, 1–14, <https://doi.org/10.1016/j.pocean.2009.07.014>, 2009.
- Gutknecht, E., Dadou, I., Marchesiello, P., Cambon, G., Le Vu, B., Sudre, J., Garçon, V., Machu, E., Rixen, T., Kock, A., Flohr, A., Paulmier, A., and Lavik, G.: Nitrogen transfers off Walvis Bay: a 3-D coupled physical/biogeochemical modeling approach in the Namibian upwelling system, *Biogeosciences*, 10, 4117–4135, <https://doi.org/10.5194/bg-10-4117-2013>, 2013.
- Hardman-Mountford, N. J. and McGlade, J. S.: Retrieval of phytoplankton biomass from ocean colour in the Benguela ecosystem, *Remote Sens. Environ.*, 79, 11–23, [https://doi.org/10.1016/S0034-4257\(01\)00236-0](https://doi.org/10.1016/S0034-4257(01)00236-0), 2002.
- Hopkins, J., Lucas, M., Dufau, C., Sutton, M., Stum, J., Lauret, O., and Channelliere, C.: Detection and variability of the Congo River plume from satellite derived sea surface temperature, salinity, ocean colour and sea level, *Remote Sens. Environ.*, 139, 365–385, <https://doi.org/10.1016/j.rse.2013.08.015>, 2013.
- Hutchings, L., van der Lingen, C. D., Shannon, L. J., Crawford, R. J. M., Verheye, H. M. S., Bartholomae, C. H., van der Plas, A. K., Louw, D., Kreiner, A., Ostrowski, M., Fidel, Q., Barlow, R. G., Lamont, T., Coetzee, J., Shillington, F., Veitch, J., Currie, J. C., and Monteiro, P. M. S.: The Benguela Current: An ecosystem of four components, *Prog. Oceanogr.*, 83, 15–32, <https://doi.org/10.1016/j.pocean.2009.07.046>, 2009.
- Johns, W. E., Brandt, P., Lumpkin, R., Fischer, J., Hormann, V., Pirani, A., Schmid, C., and Bourlès, B.: Variation of upper ocean seasonal and interannual velocity structure in the eastern equatorial Atlantic, *J. Phys. Oceanogr.*, 44, 1201–1212, <https://doi.org/10.1175/JPO-D-13-0132.1>, 2014.
- Johnson, E. S., Bonjean, F., Lagerloef, G. S., Gunn, J. T., and Mitchum, G. T.: Validation and error analysis of OSCAR sea surface currents, *J. Atmos. Ocean. Tech.*, 24, 688–701, <https://doi.org/10.1175/JTECH1971.1>, 2007.
- Jouanno, J., Marin, F., du Penhoat, Y., Sheinbaum, J., and Cole, H.: Seasonal heat balance in the upper 100 m of the equatorial Atlantic Ocean, *J. Geophys. Res.-Oceans*, 116, C9, <https://doi.org/10.1029/2010JC006912>, 2011.
- JPL MUR MEaSURES Project: GHRSSST Level 4 MUR Global Foundation Sea Surface Temperature Analysis, Ver. 4.1, PO.DAAC [data set], CA, USA, <https://doi.org/10.5067/GHGMR-4FJ04>, 2015.
- Kobayashi, S., Ota, Y., Harada, Y., Ebata, A., Mori, M., Onoda, H., Onogi, K., Kamiguchi, H., Kobayashi, C., Endo, H., Miyaoka, K., and Takahashi, K.: The JRA-55 Reanalysis: General specifications and basic characteristics, *J. Meteorol. Soc. Jpn.*, 93, 5–48, <https://doi.org/10.2151/jmsj.2015-001>, 2015.
- Kopte, R.: The Angola Current in a Tropical Seasonal Upwelling System: Seasonal Variability in Response to Remote Equatorial and Local Forcing, PhD thesis,

- Christian-Albrechts Universität Kiel, Germany, https://macau.uni-kiel.de/servlets/MCRFileNodeServlet/dissertation_derivate_00007334/20170928_dissertation_robert_kopte.pdf (last access: 11 April 2026), 2017.
- Körner, M., Brandt, P., and Dengler, M.: Seasonal cycle of sea surface temperature in the tropical Angolan Upwelling System, *Ocean Sci.*, 19, 121–139, <https://doi.org/10.5194/os-19-121-2023>, 2023.
- Körner, M., Brandt, P., Illig, S., Dengler, M., Subramaniam, A., Bachèlery, M. L., and Krahnemann, G.: Coastal trapped waves and tidal mixing control primary production in the tropical Angolan upwelling system, *Sci. Adv.*, 10, adj6686, <https://doi.org/10.1126/sciadv.adj6686>, 2024.
- Koseki, S., Cabos, W., Sein, D. V., and Mohino, E.: The role of the Gulf of Guinea upwelling in the atmospheric circulation of the tropical Atlantic in a high-resolution coupled model, *Clim. Dynam.*, 51, 1017–1035, <https://doi.org/10.1007/s00382-017-3896-2>, 2018.
- Koubanova, M., Koseki, S., and Keenlyside, N. S.: Seasonal variability of the Atlantic cold tongue and its relationship with the Angola-Benguela upwelling system, *Clim. Dynam.*, 51, 2975–2993, <https://doi.org/10.1007/s00382-018-4197-0>, 2018.
- Locarnini, M. M., Mishonov, A. V., Baranova, O. K., Boyer, T. P., Zweng, M. M., Garcia, H. E., Mishonov, A., and Smolyar, I.: World ocean atlas 2018, volume 1: Temperature, NOAA Atlas NESDIS, 52 pp., <https://archimer.ifremer.fr/doc/00651/76338/77329.pdf> (last access: 11 April 2026), 2018.
- Loukos, H. and Mémery, L.: Simulation of the nitrate seasonal cycle in the equatorial Atlantic ocean during 1983 and 1984, *J. Geophys. Res.-Oceans*, 104, 15549–15573, <https://doi.org/10.1029/1999JC900084>, 1999.
- Madec, G. and the NEMO System Team: NEMO Ocean Engine Reference Manual, Zenodo [code], <https://doi.org/10.5281/zenodo.1464816>, 2024.
- Mbang Essome, L. J., Alory, G., Dadou, I., Da-Allada, C. Y., Ngakala, R. D., and Morvan, G. L.: Physical and biological processes driving seasonal variability of Nitrate budget and biological productivity in the Gabon-Congo upwelling system. In *Ocean Science*, Zenodo [code and data set], <https://doi.org/10.5281/zenodo.19384386>, 2026.
- Messié, M. and Chavez, F. P.: Seasonal regulation of primary production in eastern boundary upwelling systems, *Prog. Oceanogr.*, 134, 1–18, <https://doi.org/10.1016/j.pocean.2014.10.011>, 2015.
- Monteiro, P., Dewitte, B., Scranton, M., Paulmier, A., and Van der Plas, A.: The role of open ocean boundary forcing on seasonal to decadal-scale variability and long-term change of natural shelf hypoxia, *Environ. Res. Lett.*, 6, 024002, <https://doi.org/10.1088/1748-9326/6/2/024002>, 2011.
- Ngakala, R. D., Alory, G., Da-Allada, C. Y., Dadou, I., Cardot, C., Morvan, G., and Balotcha, E.: Seasonal mixed layer temperature in the Congolese upwelling system, *J. Geophys. Res.-Oceans*, 130, e2023JC020528, <https://doi.org/10.1029/2023JC020528>, 2025.
- Nieto, K. and Mélin, F.: Variability of chlorophyll *a* concentration in the Gulf of Guinea and its relation to physical oceanographic variables, *Prog. Oceanogr.*, 151, 97–115, <https://doi.org/10.1016/j.pocean.2016.12.001>, 2017.
- Nubi, O., Bourles, B., and Edokpayi, C.: On the Nutrient distribution and phytoplankton biomass in the Gulf of Guinea equatorial band as inferred from In-situ measurements, *J. Oceanogr. Mar. Sci.*, 7, 1–11, <https://doi.org/10.5897/JOMS2015.0125>, 2016.
- Ostrowski, M., da Silva, J. C. B., and Bazik-Sangolay, B.: The response of sound scatterers to El Niño- and La Niña-like oceanographic regimes in the southeastern Atlantic, *ICES J. Mar. Sci.*, 66, 1063–1072, <https://doi.org/10.1093/icesjms/fsp102>, 2009.
- Radenac, M.-H., Jouanno, J., Tchamabi, C. C., Awo, M., Bourlès, B., Arnault, S., and Aumont, O.: Physical drivers of the nitrate seasonal variability in the Atlantic cold tongue, *Biogeosciences*, 17, 529–545, <https://doi.org/10.5194/bg-17-529-2020>, 2020.
- Resplandy, L., Hogikyan, A., Müller, J. D., Najjar, R. G., Bange, H. W., Bianchi, D., and Regnier, P.: A synthesis of global coastal ocean greenhouse gas fluxes, *Global Biogeochem. Cy.*, 38, e2023GB007803, <https://doi.org/10.1029/2023GB007803>, 2024.
- Richter, I.: Climate model biases in the eastern tropical oceans: Causes, impacts and ways forward, *Wires Clim. Change*, 6.3, 345–358, <https://doi.org/10.1002/wcc.338>, 2015.
- Ridgway, K. R., Dunn, J. R., and Wilkin, J. L.: Ocean interpolation by four-dimensional least squares – Application to the waters around Australia, *J. Atmos. Ocean. Tech.*, 19, 1357–1375, [https://doi.org/10.1175/1520-0426\(2002\)019<1357:OIBFDW>2.0.CO;2](https://doi.org/10.1175/1520-0426(2002)019<1357:OIBFDW>2.0.CO;2), 2002.
- Rouault, M.: Bi-annual intrusion of tropical water in the northern Benguela upwelling, *Geophys. Res. Lett.*, 39, L12606, <https://doi.org/10.1029/2012gl052099>, 2012.
- Scannell, H. A. and McPhaden, M. J.: Seasonal mixed layer temperature balance in the southeastern tropical Atlantic, *J. Geophys. Res.-Oceans*, 123, 5557–5570, <https://doi.org/10.1029/2018JC014099>, 2018.
- Schott, F. A., Fischer, J., and Stramma, L.: Transports and pathways of the upper-layer circulation in the western tropical Atlantic, *J. Phys. Oceanogr.*, 28, 1904–1928, [https://doi.org/10.1175/1520-0485\(1998\)028<1904:TAPOTU>2.0.CO;2](https://doi.org/10.1175/1520-0485(1998)028<1904:TAPOTU>2.0.CO;2), 1998.
- Siegfried, L., Schmidt, M., Mohrholz, V., Pogrzeba, H., Nardini, P., Böttinger, M., and Scheuermann, G.: The tropical-subtropical coupling in the Southeast Atlantic from the perspective of the northern Benguela upwelling system, *PLOS ONE*, 14, e0210083, <https://doi.org/10.1371/journal.pone.0210083>, 2019.
- Sikhakolli, R., Sharma, R., Basu, S., Gohil, B. S., Sarkar, A., and Prasad, K. V. S. R.: Evaluation of OSCAR ocean surface current product in the tropical Indian Ocean using in situ data, *J. Earth Syst. Sci.*, 122, 187–199, <https://doi.org/10.1007/s12040-012-0258-7>, 2013.
- Sowman, M. and Cardoso, P.: Small-scale fisheries and food security strategies in countries in the Benguela Current Large Marine Ecosystem (BCLME) region: Angola, Namibia and South Africa, *Mar. Policy*, 34, 1163–1170, <https://doi.org/10.1016/j.marpol.2010.03.016>, 2010.
- Tchupalanga, P., Dengler, M., Brandt, P., Kopte, R., Macueria, M., Coelho, P., Ostrowski, M., and Keenlyside, N. S.: Eastern Boundary Circulation and Hydrography Off Angola: Building Angolan Oceanographic Capacities, *B. Am. Meteorol. Soc.*, 99, 1589–1605, <https://doi.org/10.1175/Bams-D-17-0197.1>, 2018.
- Thiam, A., Alory, G., Jouanno, J., Da-Allada, C. Y., and Morvan, G.: Coastal upwelling in the Northern Gulf of Guinea: Seasonal cycle and mesoscale interactions, *Ocean Model.*, 188, 102300, <https://doi.org/10.1016/j.ocemod.2024.102300>, 2024.

- Tilstone, G., Smyth, T., Poulton, A., and Hutson, R.: Measured and remotely sensed estimates of primary production in the Atlantic Ocean from 1998 to 2005, *Deep-Sea Res. Pt. II*, 56, 918–930, <https://doi.org/10.1016/j.dsr2.2008.10.034>, 2009.
- Topé, G. D. A., Alory, G., Djakouré, S., Da-Allada, C. Y., Jouanno, J., and Morvan, G.: How does the Niger River warm coastal waters in the Northern Gulf of Guinea?, *Front. Mar. Sci.*, 10, 1187202, <https://doi.org/10.3389/fmars.2023.1187202>, 2023.
- Tuchen, F. P., Brandt, P., Lübbecke, J. F., and Hummels, R.: Transports and pathways of the tropical AMOC return flow from Argo data and shipboard velocity measurements, *J. Geophys. Res.-Oceans*, 127, e2021JC018115, <https://doi.org/10.1029/2021JC018115>, 2022.
- Voldoire, A., Belamari, S., and Lévy, M.: On the role of ocean-atmosphere interaction in the onset of the Atlantic cold tongue, *Clim. Dynam.*, 53, 5437–5455, <https://doi.org/10.1007/s00382-019-04717-0>, 2019.
- Xu, Z., Li, M., Patricola, C. M., and Chang, P.: Oceanic origin of southeast tropical Atlantic biases, *Clim. Dynam.*, 43, 2915–2930, <https://doi.org/10.1007/s00382-013-1901-y>, 2014.
- Zeng, Z., Brandt, P., Lamb, K. G., Greatbatch, R. J., Dengler, M., Claus, M., and Chen, X.: Three-dimensional numerical simulations of internal tides in the Angolan upwelling region, *J. Geophys. Res.-Oceans*, 126, e2020JC016460, <https://doi.org/10.1029/2020JC016460>, 2021.
- Zuidema, P., Redemann, J., Haywood, J., Wood, R., Piketh, S., Hipondoka, M., and Formenti, P.: Smoke and clouds above the southeast Atlantic: Upcoming field campaigns probe absorbing aerosol's impact on climate, *B. Am. Meteorol. Soc.*, 97, 1131–1135, <https://doi.org/10.1175/BAMS-D-15-00032.1>, 2016.
- Zweng, M. M., Seidov, D., Boyer, T. P., Locarnini, M., Garcia, H. E., Mishonov, A. V., and Smolyar, I.: World ocean atlas 2018, volume 2: Salinity, NOAA Atlas NESDIS, 82, https://www.ncei.noaa.gov/data/oceans/woa/WOA18/DOC/woa18_vol2.pdf (last access: 11 April 2026), 2019.